Introduction to Circuit Quantum Electrodynamics

CSC 269Q: Quantum Computer Programming
Stanford University, Spring, 2019

by
Matthew James Reagor

Contents

CHAPTER 1

Introduction to Circuit QED

Circuit Quantum Electrodynamics (cQED) is a toolbox for implementing nontrivial quantum circuits that can be precisely designed and controlled. We begin this chapter by putting the quantum mechanics of circuits on solid theoretical footing. We first describe how the circuit operators of voltage and flux can be quantized. Then, the theoretical framework of the Josephson effect and its realization as a nonlinear circuit element is introduced. Finally, we show how circuits coupled with Josephson elements can achieve QED effects.

This chapter benefits from a long history of excellent theses and pedagogical reviews on the subject of Josephson quantum circuits. In particular, the beginning of this chapter closely follows the seminal work by Devoret [1] and especially the recent treatment by Girvin [2]. We rely on this foundation to advance a modern description of QED as a natural consequence the Josephson effect beginning in Section 1.3.2. By treating our cQED system as a 'Black Box' [3], we are able to describe driven, coupled, nonlinear, quantum circuits with a single framework. The consequence (Section 1.4) is an intuitive set of quantum behaviors and 'selection rules' for a circuit that can potentially possess many degrees of freedom.

In order to explore the rich behavior of a single cQED system (an otherwise-linear circuit with one Josephson element), this chapter does not review the many other types of

quantum circuits or superconducting qubits in detail. For this purpose, we refer the reader to the reviews by Clarke and Wilhelm [4] and also the review by Devoret and Schoelkopf [5].

1.1 Building blocks of cQED

Circuits made of capacitors and inductors have equivalent descriptions in mechanical systems of masses and springs. We use that analogy throughout this section to justify our intuition and make connections to other experimental techniques. For instance, voltage (V) and flux (Φ) are collective phenomena. Typically in a circuit, a countless number of charge carriers generate our measured V or Φ. Fortunately, we are able to abstract away the microscopic forces that act on these solid-state charge carriers. This is analogous to treating a many-atom chunk of material as a single mass with a single momentum: as long as the inter-mass dynamics (lattice vibrations) occur at a sufficiently high frequency, we can approximate these modes to be their ground state. Indeed, for aluminum circuits, the equivalent modes (plasma oscillations of free charge carriers) occur at frequencies above $\omega/2\pi \gtrsim 10^{15}$ Hz [6], five orders of magnitude higher frequencies than we consider here in this thesis. The collective motion approximation is therefore well justified.

Superconductivity plays the vital role of suppressing dissipation in our circuits. Perhaps more importantly, an ideal superconductor also gives us access to a dissipationless nonlinear circuit element, which we describe in Section 1.2. In both of these cases, the gap of the superconductor (Δ) gives us another ground state to consider, allowing more rigor to the collective motion approximation [7]. The gap of our circuit's superconductor also sets a limit to the temperatures and excitation energies that can be used [7]. The frequencies associated with the break down of superconductivity are much smaller than the onset of plasma oscillations considered above. When working with aluminum for instance, drives above $\omega/2\pi \gtrsim 2\Delta/h$ ($\approx 80 - 100$ GHz for aluminum) can efficiently excite quasiparticles above the gap.

Our operating frequencies are bounded below by the requirement that our resonant circuits be in their quantum mechanical ground states. To achieve a Boltzmann factor suppression of the first excited state to approximately one percent, we require then that $\omega/2\pi \gtrsim 5k_BT$. At the operating temperatures of a commercial dilution refrigerator ($T \sim 20$ mK), that requirement translates to $\omega/2\pi \gtrsim 2$ GHz. These considerations therefore place our quantum circuits squarely in the microwave domain.

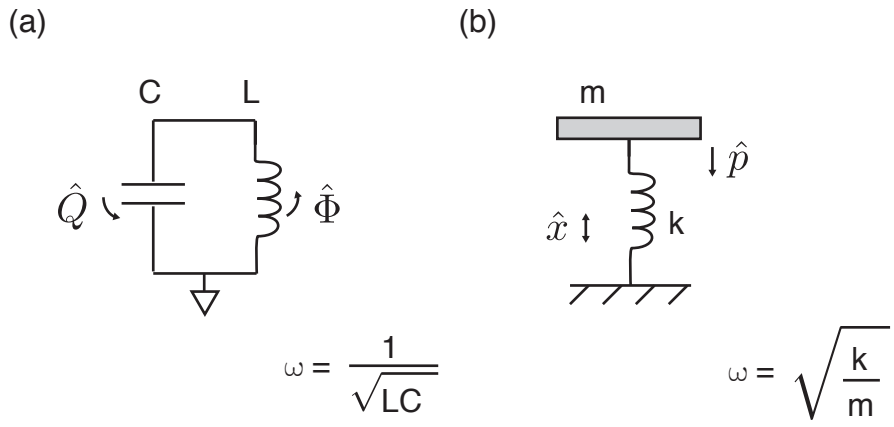

Figure 1.1: Quantum harmonic oscillators. **(a)** An electrical harmonic oscillator is constructed by placing a capacitor (C) in parallel with an inductor (L). The conjugate variables that describe the resulting oscillation are the charge on the capacitor $\hat{Q}$ and flux through the inductor $\hat{\Phi}$. The natural frequency of this oscillator is related to these two circuit elements by $\omega = 1/\sqrt{LC}$. **(b)** The analogous mechanical circuit to the LC oscillator is a simple mass-spring system with mass m and inverse-spring constant k^{-1}. In this oscillator, the displacement of the spring $\hat{x}$ and the momentum of the mass $\hat{p}$ form the equivalent conjugate variables to the system as charge and flux in the electrical circuit. The mechanical oscillator has the resonant frequency $\omega = \sqrt{k/m}$.

1.1.1 The quantized circuit

To quantize a circuit we proceed in the canonical fashion [1, 2] by finding a Hamiltonian for the system and its conjugate variables, which will become our quantum operators. The foundational circuit to this thesis is the linear oscillator (Fig. 1.1). This circuit combines a capacitor (C) in parallel with an inductor (L). On resonance, energy sloshes between a charging energy ($E_C = Q^2/2C$) and an inductive energy ($E_L = \Phi^2/2L$). For the mass-spring system, energy likewise oscillates between kinetic energy ($p^2/2m$) and potential energy ($x^2/2k^{-1}$). Combining the circuit's kinetic energy (E_C) and potential energy (E_L) terms to form a Lagrangian [2] gives

$$\mathcal{L} = \frac{Q^2}{2C} - \frac{\Phi^2}{2L}. \tag{1.1}$$

Because these elements share a node in the circuit, we can use the flux-voltage relation [1]

$$\Phi(t) \equiv \int_{-\infty}^{t} V(\tau)d\tau = \int \frac{Q(\tau)}{C}d\tau \tag{1.2}$$

to rewrite the charging energy as

$$\mathcal{L} = \frac{C\dot{\Phi}^2}{2} - \frac{\Phi^2}{2L}. \tag{1.3}$$

We recognize that flux through the inductor ($\Phi = L\dot{Q}$) is the conjugate variable of charge [2], since

$$\frac{\delta\mathcal{L}}{\delta\dot{\Phi}} = L\dot{Q} = \Phi. \tag{1.4}$$

Therefore, we have a classical Hamiltonian for this circuit that is

$$H = \Phi\dot{Q} - \mathcal{L} = \frac{\Phi^2}{2L} + \frac{Q^2}{2C}. \tag{1.5}$$

Now, we are now ready convert these variables to quantum mechanical operators (e.g. $\Phi \Rightarrow \hat{\Phi}$) and the Hamiltonian as well ($H \Rightarrow \hat{H}$). Additionally, we can factor Equation 1.5, using

$$\hat{x}^2 + \hat{y}^2 = (\hat{x} + \imath\hat{y})(\hat{x} - \imath\hat{y}) - \imath\left[\hat{x}, \hat{y}\right] \tag{1.6}$$

to eventually simplify our circuit's description, now giving

$$\hat{H} = \left(\frac{\hat{\Phi}}{\sqrt{2L}} + \imath\frac{\hat{Q}}{\sqrt{2C}}\right)\left(\frac{\hat{\Phi}}{\sqrt{2L}} - \imath\frac{\hat{Q}}{\sqrt{2C}}\right) - \frac{\imath}{2\sqrt{LC}}\left[\hat{Q}, \hat{\Phi}\right]. \tag{1.7}$$

The conjugate relationship between flux and charge in Equation 1.4 gives us the commutation rules for free as $\left[\hat{Q}, \hat{\Phi}\right] = -\imath\hbar$ [1]. The symmetric form of Equation 1.7 suggests defining a simpler operator $\hat{a}$ such that

$$\hat{a} = \frac{1}{\sqrt{\hbar\omega}}\left(\frac{\hat{\Phi}}{\sqrt{2L}} - \imath\frac{\hat{Q}}{\sqrt{2C}}\right), \tag{1.8}$$

where $\omega \equiv 1/\sqrt{LC}$. This substitution wonderfully allows us to recast the Hamiltonian [2] as

$$\hat{H} = \hbar\omega\left(\hat{a}^\dagger\hat{a} + \tfrac{1}{2}\right). \tag{1.9}$$

We recognize this Hamiltonian as a simple harmonic oscillator with a frequency ω, and

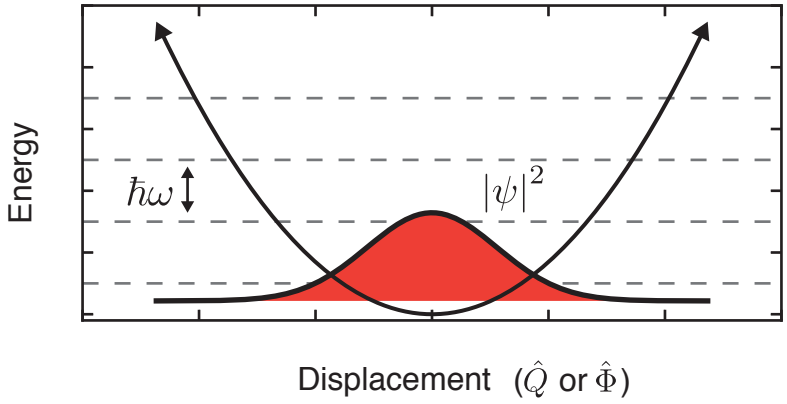

Figure 1.2: Energy levels of the quantum harmonic oscillator. The quadratic potential yields evenly spaced energy eigenstates ($\Delta E = \hbar\omega$). The ground state of the system is Gaussian distributed in the conjugate variables of motion, e.g. charge $\hat{Q}$ and flux $\hat{\Phi}$. Note that the circuit has finite probability $|\psi|^2$ of being detected at a nonzero value of $\hat{Q}$ or $\hat{\Phi}$ for the ground state. This phenomenon is known as zero-point fluctuations of the circuit and leads to a number of important consequences as we see in this chapter.

where the operator $\hat{a}$ is the annihilation operator and $\hat{a}^\dagger\hat{a} = \hat{n}$, the number operator. Further, we can invert Equation 1.8 and its Hermitian conjugate [2] to rewrite the flux through the inductor and charge on the capacitor as

$$\hat{\Phi} = \sqrt{\frac{\hbar Z}{2}}\left(\hat{a}^\dagger + \hat{a}\right) \tag{1.10a}$$

$$\hat{Q} = -\imath\sqrt{\frac{\hbar}{2Z}}\left(\hat{a}^\dagger - \hat{a}\right), \tag{1.10b}$$

where $Z = \sqrt{L/C}$ is the impedance of the circuit.

It is worth pointing out that the relationship between circuits and mechanical degrees of freedom is more than an analogy. The first experiments to explore the ideas of Quantum Non-Demolition (QND) measurements were attempts to observe gravitational waves in the excitation of massive mechanical oscillators, transduced by LC oscillators [8] as

$$\hat{H} = \frac{\hat{p}^2}{2m} + \frac{1}{2}m\hat{x}^2 + \frac{\hat{\Phi}^2}{2L} + \frac{\hat{Q}^2}{2C} + \hbar g\hat{x}\hat{Q}. \tag{1.11}$$

where the term interaction term $\hat{H}_{int} = \hbar g \hat{x} \hat{Q}$ is created by the mass being suspended between two plates of a capacitor; displacing the mass changes the capacitor's charge distribution. Today, electromechanical systems are exploiting this coupling term in to explore the quantum dynamics of massive objects [9].

We now turn to solving for the ground state of the LC oscillator, which will prepare us for studying driven circuits in Section 1.1.3 and nonlinear LC systems in Section 1.3.

1.1.2 Gaussian states in an LC oscillator

As for all harmonic oscillators, our circuit acquires non-zero variance of charge and flux, even in its ground state, i.e.

$$\langle 0|\hat{\Phi}^2|0\rangle \equiv \Phi_{\mathrm{ZPF}}^2 \neq 0. \tag{1.12}$$

These zero-point fluctuations can be related to the flux quantum ($\Phi_0 \equiv h/2e$) and the resistance quantum ($R_{\mathrm{Q}} \equiv h/2e^2$) [1] as

$$\Phi_{\mathrm{ZPF}} = \Phi_0 \sqrt{\frac{Z}{2\pi R_{\mathrm{Q}}}} \tag{1.13a}$$

$$Q_{\mathrm{ZPF}} = e \sqrt{\frac{R_{\mathrm{Q}}}{2\pi Z}}. \tag{1.13b}$$

The circuit's impedance therefore determines the relative strength of these fluctuations. We recognize in Equation 1.13 that a low impedance circuit has less flux noise but more charge noise.

The shape of ground state wave function ($|\psi_0\rangle$) is interesting as well [10]. If we make use of the differential operator in quantum mechanics, e.g. $\hat{Q} = -\imath\hbar\,(\partial/\partial\Phi)$, then the statement $\hat{a}|\psi_0\rangle = 0$ can be written as

$$\left(\frac{\Phi}{\sqrt{2L}} + \frac{\hbar}{\sqrt{2C}}\frac{\partial}{\partial\Phi}\right)|\psi_0(\Phi, Q)\rangle = 0. \tag{1.14}$$

A similar expression holds for Q, and both of these equations have a Gaussian solution. When normalized, this gives for the ground state

$$|\psi_0(\Phi, Q)\rangle = \frac{1}{\sqrt{2\pi\Phi_{\mathrm{ZPF}}Q_{\mathrm{ZPF}}}} \times e^{-(\Phi^2/4\Phi_{\mathrm{ZPF}}^2 + Q^2/4Q_{\mathrm{ZPF}}^2)} \tag{1.15}$$

Because the Gaussian distribution is normalized by the zero-point fluctuations, it is often

convenient to describe the circuit in a dimensionless quadrature representation as

$$\hat{X} \equiv \frac{1}{\sqrt{\hbar Z}} \times \hat{\Phi} = \frac{1}{\sqrt{2}} \left(\hat{a} + \hat{a}^\dagger\right) \tag{1.16a}$$

$$\hat{Y} \equiv \sqrt{\frac{Z}{\hbar}} \times \hat{Q} = -\imath \frac{1}{\sqrt{2}} \left(\hat{a} - \hat{a}^\dagger\right), \tag{1.16b}$$

such that which simplifies the wave function of the ground state to a highly symmetric two-dimensional Gaussian form

$$|\psi_0(X,Y)\rangle = \frac{1}{\sqrt{2\pi}} \times e^{-(X^2+Y^2)/4}. \tag{1.17}$$

The ground state is only one eigenvector of $\hat{a}$. Actually, there are infinitely many such solutions of the form

$$\hat{a}\,|\psi\rangle = \alpha\,|\psi\rangle \tag{1.18}$$

where α is a complex number. All of these wavefunctions are Gaussian distributed in (X,Y) with the same standard deviation as the ground state, but have some displaced centroid $(X_0, Y_0) = (\Re(\alpha), \Im(\alpha))$ as

$$|\psi(X,Y)\rangle = \frac{1}{\sqrt{2\pi}} \times e^{-((X-X_0)^2+(Y-Y_0)^2)/4}. \tag{1.19}$$

These states are given the name coherent states [11], and such states play a number of important roles in this thesis.

We can use the eigenvector relation (Eq. 1.18) to learn about the photon statistics of a coherent state. In particular, knowing the complex eigenvalue α gives us the ability to exactly describe the distribution of the state across the entire Hilbert space of the mode. To see how, we begin by stating the eigenvalue relationship more precisely in Fock-space [10],

$$\hat{a}\,|\alpha\rangle = \hat{a} \sum_n C_n\,|n\rangle = \alpha\,|\alpha\rangle\,. \tag{1.20}$$

Using the definition of the annihilation operator, $\hat{a}\,|n\rangle = \sqrt{n}\,|n-1\rangle$, we have that

$$C_n = \frac{\alpha}{\sqrt{n}} C_{n-1} = \frac{\alpha^2}{\sqrt{n(n-1)}} C_{n-2} = \ldots = \frac{\alpha^n}{\sqrt{n!}} C_0. \tag{1.21}$$

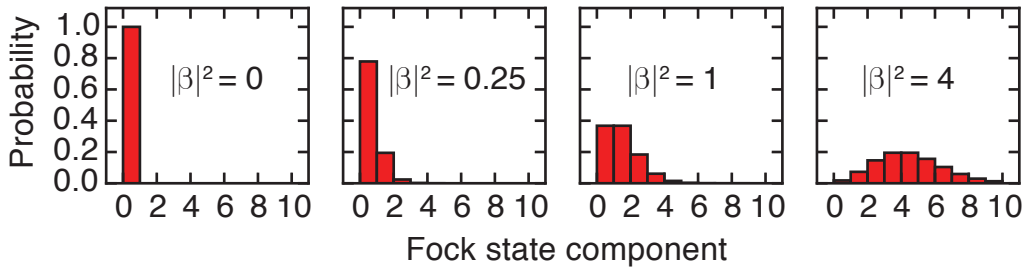

Figure 1.3: Photon number statistics of coherent states. The probability of the oscillator to contain exactly n photons (P_n) for coherent states of amplitude β is a discrete Poisson distribution, truncated here for visibility at $N = 10$. The distribution broadens at larger displacements since the variance is equal to the mean number of photons $|\beta|^2$.

Then, we can express the coherent state in the Fock basis as

$$|\alpha\rangle = \exp(-|\alpha|^2/2) \sum_n \frac{\alpha^n}{\sqrt{n!}} |n\rangle, \tag{1.22}$$

where the normalization factor is found by the constraint that $\sum |C_n|^2 = 1$Equation 1.22 can be used to calculate any expectation value of the field quadratures. For instance, the probability of detecting a coherent state in a specific Fock state $|m\rangle$ (P_m) is Poisson distributed as

$$|C_m|^2 = \exp(-|\alpha|^2) \frac{|\alpha|^{2m}}{m!}. \tag{1.23}$$

The mean photon number $\bar{n}$ can also be calculated from the distribution of P_m to be

$$\bar{n} \equiv \langle \alpha | \hat{a}^\dagger \hat{a} | \alpha \rangle = |\alpha|^2. \tag{1.24}$$

Equation 1.20 can further be used to show that two coherent states also have a variance of their number distribution $\Delta n^2 = \bar{n}$; that such states minimize quadrature uncertainties ($\Delta X^2 \Delta Y^2 = 1/4$); and that they form an overcomplete set of states on the Hilbert space of the mode.

In the next subsection, we describe how these states are the natural consequence of classical drives.

1.1.3 Arbitrary classical drives on linear circuits

In this section, we consider the effect of an arbitrary, but linear, classical drive on an LC oscillator. Such a drive can only take a coherent state in the oscillator, e.g. its ground state, to another coherent state [12]. That transformation be can described by a unitary operator, called the displacement operator [11],

$$\hat{D}(\alpha)|0\rangle = |\alpha\rangle, \tag{1.25}$$

where α is the amplitude of the displacement and $|\alpha|^2$ is the resulting average photon occupancy.

A derivation for the form of the displacement operator that is particularly useful for our purposes is given by Girvin [2]. Consider that, as discussed in Section 1.1.2, any coherent state is equivalent to the vacuum state up to a transformation of coordinate systems. Therefore, a finite amplitude coherent state is at the origin of some X', Y' plane. We have confidence then that we can obtain a precise description of $\hat{D}(\alpha)$ by requiring that this operator offsets the coordinate system of a state by $-\alpha$ but otherwise leaves it unaffected. Following Girvin, for this type of transformation, we can use Taylor's theorem that for a function of one variable

$$f(x) = f(a) + f'(a)\,(x-a) + \frac{f''(a)}{2}\,(x-a)^2 + ... \tag{1.26}$$

Furthermore, we can express this infinite series equivalently as an exponentiated differential operator, a form attributed to Lorentz, as

$$f(x) = e^{(x-a)\frac{d}{dx}} f(x)\Big|_{x=a}. \tag{1.27}$$

For a given initial state wave function, $|\beta\rangle$, transforming the coordinates by $\hat{X} \Rightarrow \hat{X} - \alpha$ can be written explicitly [2] as

$$\hat{D}(\alpha)|\beta\rangle = \exp(-\alpha\frac{d}{dX})|\psi(X)\rangle\Big|_{X=\beta}. \tag{1.28}$$

We use that $Y = (\imath/2)(d/dX)$ to write the displacement operator as

$$\hat{D}(\alpha)|\beta\rangle = \exp(-2\imath\alpha\hat{Y})|\beta\rangle = \exp(-\alpha(\hat{a} - \hat{a}^\dagger))|\beta\rangle. \tag{1.29}$$

We can show a number of interesting properties about $\hat{D}$, but perhaps the most important is to check that $\hat{D}$ on the vacuum state produces the correct coherent state. We rewrite the displacement operator in a more convenient form $\hat{D}(\alpha) = \exp(-|\alpha|^2)\exp(+\alpha\hat{a}^\dagger)\exp(-\alpha\hat{a})$ [11]. Since $\hat{a}|0\rangle = 0$, we only have to keep the $\hat{a}^\dagger$ terms:

$$\hat{D}(\alpha)|0\rangle = \exp(-|\alpha|^2)\exp(+\alpha\hat{a}^\dagger)|0\rangle, \tag{1.30}$$

and we use a Taylor series in the exponentiated operator [10] to yield

$$\begin{aligned}\hat{D}(\alpha)|0\rangle &= \exp(-|\alpha|^2)\sum_n \frac{\left(+\alpha\hat{a}^\dagger\right)^n}{n!}|0\rangle \\ &= \exp(-|\alpha|^2)\sum_n \frac{\alpha^n}{\sqrt{n!}}|n\rangle\end{aligned} \tag{1.31}$$

which is indeed the same form for $|\alpha\rangle$ as Equation 1.22.

A formal proof that Gaussian states of circuits are only trivially affected by an arbitrary drive is adapted from [12] in Appendix **??**. However, an intuitive toy model is as follows. Consider an arbitrary current source coupled to the flux of our inductor as shown in Figure 1.4. The evolution of the circuit will be governed by

$$\hat{H}(t) = \hbar\omega\hat{a}^\dagger\hat{a} - I(t)\hat{\Phi} = \hbar\epsilon(t)\hat{\Phi} \tag{1.32}$$

where we have introduced ϵ in order to work with more convenient units. We proceed by taking a rotating frame to remove the harmonic oscillator term [13], leaving

$$\hat{H}_1(t) = \hbar\epsilon(t)\tilde{\Phi}, \tag{1.33}$$

where now $\tilde{\Phi}$ has rotating ladder operators $\tilde{a} = \hat{a}e^{-\imath\omega t}$.

Any physical drive, i.e. presenting finite dissipation to the circuit, will result in a drive that is a differentiable function. Therefore, we can find an infinitesimally small time δt over which the Hamiltonian is approximately time independent. The circuit, initialized in some coherent state $|\beta_0\rangle$, will therefore evolve via the unitary propagator

$$|\beta_{\delta t}\rangle = \hat{U}_{drive}|\beta_0\rangle \approx e^{-\imath\hat{H}\delta t/\hbar}|\beta_0\rangle = e^{-\imath\epsilon_0\delta\tilde{\Phi}}|\beta_0\rangle \tag{1.34}$$

Under these conditions, the propagator is cast as a displacement operator with $\delta\alpha = \epsilon_0\delta t$. Then, the tilde on $\hat{\Phi}$ simply determines the angle of the displacement. Taking many

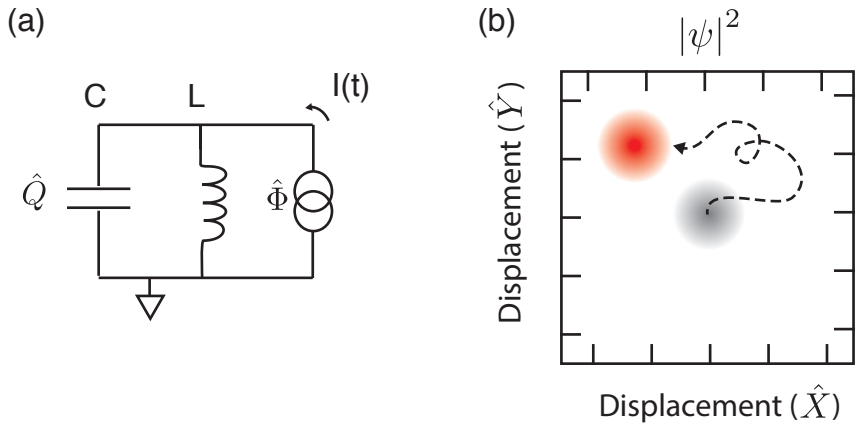

Figure 1.4: Effect of an arbitrary drive on a damped oscillator. (a) An LC oscillator is biased with a time-dependent current drive. Here, damping is provided by the finite input impedance of the current source. The driving current couples to the conjugate flux variable to add a potential to the system as $\hat{H}_{drive}(t) = -I(t)\hat{\Phi}$. The resulting state of the resonator can be shown to be a coherent state for all times. **(b)** The probability of detecting the oscillator at a given displacement ($\hat{X}$,$\hat{Y}$) is shown (red) for a given trajectory of $I(t)$. The linear bias pushes the oscillator from its ground state (grey) to some coherent state $|\beta\rangle$. However, at all times this trajectory can be equally described by displacing the origin of the resonator along the dashed line. The oscillator remains in its ground state while the axes $\hat{X}, \hat{Y}$ are translated. Nonlinearity is needed in the system to create more interesting states.

snapshots of this process, we can build up the trajectory of an arbitrary drive. Furthermore, we will always be stuck in a minimum uncertainty Gaussian state that resembles the quantum vacuum.

In the next section, we meet our first nonlinear circuit element, the Josephson junction. Such an element allows for even simple drives to generate states of our circuit that exhibit striking quantum mechanical properties, markedly different than the simple noise addition of the uncertainty principle.

1.2 Josephson junctions

A Josephson tunnel junction is created by sandwiching a thin insulating layer between two superconductors [14]. Supercurrents tunneling between the two superconductors obey the

Josephson equations [7, 15]. In particular, the current and voltage across the barrier is related to the phase difference between the two superconductors (δ) as

$$I = I_0 \sin\varphi \tag{1.35a}$$

$$\frac{d\varphi}{dt} = \frac{2\pi V}{\Phi_0} \tag{1.35b}$$

where the constant of proportionality I_0 is the critical current of the junction. We will describe later how such tunnel junctions are made in the practice (Section ??). For now, we focus on the new types of circuits we can make with this element.

1.2.1 Nonlinear inductance

Clearly, the Josephson relations are nonlinear. To see how such a junction can act like an inductor, consider the definition of inductance, $L \equiv V/\dot{I}$. Taking the time-derivative of the current-phase relation (Eq. 1.35a) gives

$$\frac{dI}{dt} = I_0 \cos\phi \times \frac{d\varphi}{dt} = \frac{2\pi I_0 V}{\Phi_0} \cos\varphi \tag{1.36}$$

where we have used the second Josephson relation (Eq. 1.35b) to compute the time-derivative of the phase [1]. These simple calculations allow us to define the Josephson inductance L_J as

$$L_J = \frac{\Phi_0}{2\pi I_0 \cos\varphi}. \tag{1.37}$$

Often, the $\cos\varphi$ term is ignored to quote a 'Josephson inductance' value for a given tunnel junction (L_0) in nH. For the typical devices we will discuss in this chapter, $L_0 \approx 1-10\,\text{nH}$.

Many quantum circuits make use of the full sinusoidal capabilities provided by the Josephson effect [16, e.g. and references therein]. However, we restrict ourselves in this thesis to the small phase ($\varphi \ll 1$) limit. In that limit, we have an inductance that is approximately

$$L_J \approx \frac{\Phi_0}{2\pi I_0}\left(1 + \frac{\varphi^2}{2} + \mathcal{O}(\phi^4)\right). \tag{1.38}$$

The effective inductance of a Josephson junction increases at higher phase bias. This is shown schematically in Figure 1.5. We could imagine constructing an LC oscillator using such a circuit element as the inductor. Then, the resonant frequency of the circuit should

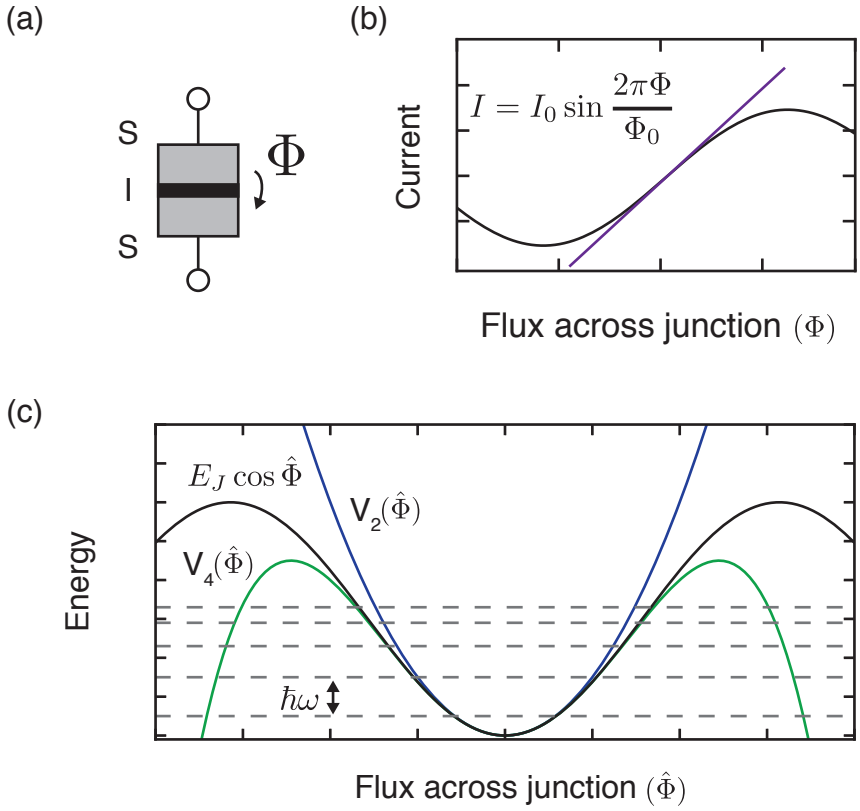

Figure 1.5: Josephson effect as a circuit element. (a) A Josephson junction is formed by separating two superconducting electrodes by a small layer of insulating material. The resulting junction serves as a nonlinear circuit element. **(b)** The current-flux relationship of the Josephson effect is sinusoidal. We can ascribe an inductance to our new circuit element as $L_J \equiv \Phi/I$, which is linear to first order (purple). At larger values of Φ the linear term over-estimates the inductance of the junction. **(c)** The basic sinusoidal potential leads to low-lying energy states that have an anharmonic spectrum. The successive approximations to this potential are a quadratic $V_2(\hat{\Phi})$ and quartic $V_4(\hat{\Phi})$ Hamiltonian terms described in this chapter.

depend on amount of energy circulating in it. Remarkably, that intuition describes the quantum properties of such a circuit, as we will see next.

1.2.2 Quantized Josephson effects

It is often more convenient to work in the flux basis when evaluating the behavior of the Josephson element [1]. We can equally describe the phase across the junction as a flux

$$\Phi = \Phi_0 \varphi. \tag{1.39}$$

We can then quantize phase on an equal footing to charge and flux as before, i.e. $\hat{\varphi} = \hat{\Phi}/\Phi_0$ [1]. Furthermore, the energy added to our system by a current and voltage at a junction is given by $\Phi_0 I$, or

$$\hat{H}_J = -E_J \cos\left(\hat{\Phi}/\Phi_0\right), \tag{1.40}$$

where

$$E_J = \frac{\Phi_0^2}{2\pi L_0} \tag{1.41}$$

is the Josephson energy. In the small flux limit limit ($|\langle\hat{\Phi}\rangle| \ll \Phi_0$), we can expand the cosine Hamiltonian of the Josephson junction in higher order operator terms with rapidly decreasing magnitude [3], as

$$\hat{H}_J \approx E_J \left[1 - \frac{1}{2}\left(\frac{\hat{\Phi}}{\Phi_0}\right)^2 + \frac{1}{4!}\left(\frac{\hat{\Phi}}{\Phi_0}\right)^4 + ...\right] \tag{1.42}$$

The small flux limit is satisfied for

$$\bar{n}\frac{\Phi_{\mathrm{ZPF}}}{\Phi_0} \ll 1. \tag{1.43}$$

Recalling that $\Phi_{\mathrm{ZPF}} \propto \sqrt{Z}$ (Eq. 1.13), we see that this limit can be satisfied for small impedances in addition to small $\bar{n}$.

In the next section, we will see that the fourth order term in this expansion is sufficient to give an LC oscillator full Hilbert state addressability [3], alleviating the problems of simple harmonic circuits.

1.3 Quantum Josephson circuits

This thesis relies on the nonlinearity of Josephson elements to address individual transitions of quantized circuits as if they were artificial atoms [17, e.g. and references therein] . The many other uses of Josephson junction circuits for quantum mechanical applications, such

as quantum limited amplifiers [18, e.g.], lossless frequency converters [19], or reconfigurable circulators [20], is beyond the scope of this chapter.

In addition, we will describe a single type of Josephson atom, the transmon, in detail. However, there are many other realizations of artificial atoms using Josephson circuits. We refer the reader to the reviews in [4, 5, and references therein] for information about these devices.

1.3.1 Black Box Quantization of a Josephson circuit

One of the simplest Josephson circuits is shown in Figure 1.6. A clever scheme to approximately diagonalize this circuit by leveraging the small-phase limit was introduced by Nigg [3] and is called Black Box Quantization (BBQ). For the circuit in Figure 1.6, the small-phase limit is equivalent to the large-capacitance limit since $Z \propto C^{-1/2}$. The idea in [3] is to treat the linear part of the junction and accompanying circuit ($\hat{H}_0$) separately from the nonlinear part of the junction ($\hat{H}_{nl}$). We proceed by finding the normal modes of the circuit (ω_0's) and then introducing the nonlinearity later as a perturbation. More precisely,

$$\hat{H} = \frac{\hat{\Phi}^2}{2L} + \frac{\hat{Q}^2}{2C} + \hat{H}_{nl} = \hbar\omega_0 \hat{a}^\dagger \hat{a} + \hat{H}_{nl}, \tag{1.44}$$

where the nonlinear part of the Hamiltonian ($\hat{H}_{nl}$) is given by

$$\hat{H}_{nl} = E_J \left[1 - \cos(\hat{\varphi})\right] - \frac{E_J}{2}\varphi^2. \tag{1.45}$$

It is important to note that up to charging effects (see Section 1.3.2), Equation 1.44 is still exact. From here, treating the nonlinearity as a perturbation will be a powerful tool to solving the dynamics of our circuit. In particular, Equation 1.43 gives a prescription for how many terms in this expansion we need to keep. The majority of thesis, and also the majority of cQED, concerns the lowest order terms in the nonlinear Hamiltonian [21], terms proportional to φ^4. However, at the conclusion of this chapter, we show how the neglected terms can be enhanced.

The circuit in Figure 1.6 is an ideal transmon artificial atom [22]. In the next section, we show show how the nonlinearity of the Josephson junction allows us to address its individual levels and later, how to operate the transmon as a qubit [21, 23].

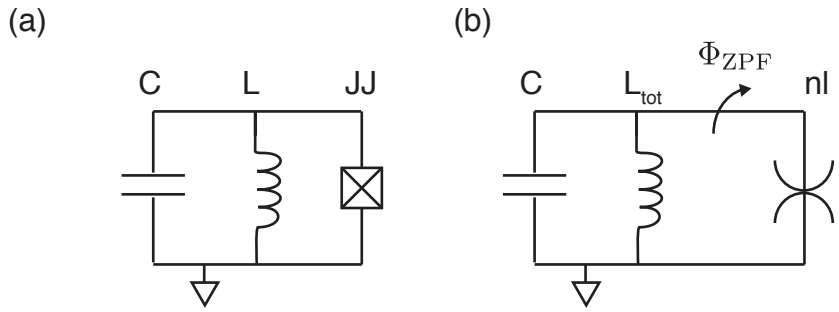

Figure 1.6: Quantizing the Josephson LC oscillator. **(a)** A parallel LC oscillator is shunted by the nonlinear admittance of a Josephson junction (box element). **(b)** The effect of the Josephson junction is separated into two components, the linear term is absorbed into the the total inductance of the LC oscillator, and a new element is introduced (spider element) that contains only the nonlinear terms of the junction's response to flux ($\hat{H}_{\rm nl}$) [3]. The solution to the Hamiltonian is determined, up to a scaling term E_J, by the magnitude of zero point fluctuations in the flux variable, or equivalently, the impedance of the LC resonator, provided that the charging energy is negligible.

1.3.2 Transmon artificial atoms

The circuit in Fig. 1.6 is susceptible to low-frequency charge offsets since the junction presents a high impedance tunnel barrier to unpaired electrons. This offset charge shifts the total charge operator by $\hat{Q} \Rightarrow \hat{Q} + Q_{ofs}$ in Equation 1.44. The perturbation ($\hat{H}_Q$) on the Hamiltonian is two new terms

$$\hat{H}_Q = \frac{(\hat{Q}+Q_{ofs})^2}{2C} - \frac{\hat{Q}^2}{2C} = \left(\frac{Q_{ofs}}{C}\right)\hat{Q} + \frac{(Q_{ofs})^2}{2C}. \tag{1.46}$$

The first term on the right hand side of the final expression accounts for the static voltage induced by the offset charge. The second is a renormalization of the energy that could be discarded, unless the offset charge is fluctuating, which is always observed experimentally [24, e.g.]. Charge fluctuations cause dephasing for our circuit. These effects can be solved for analytically, as discussed in detail [22], but, by working in the large capacitance limit, we become exponentially insensitive to these charge offsets. This limit, where

$$E_J \gg Q_{ofs}^2/2C \sim e^2/2C \equiv E_C, \tag{1.47}$$

is called the transmon limit. For $E_J \lesssim E_C$, this is known as a Cooper Pair Box (CPB) charge qubit [25] and is sensitive to charge noise.

1.3.3 Driving a transmon atom

What is the fate of our nonlinear circuit under the drive we considered for the LC oscillator in Section 1.1.3? The total Hamiltonian for the driven transmon atom is similar to original expression (Eq.1.32), except with the addition of an $\hat{H}_{nl}$ term (Eq. 1.45) of the junction. Now, the driven system evolves under

$$\hat{H} = \hbar\omega\hat{a}^\dagger\hat{a} - \hbar\epsilon(t)(\hat{a} + \hat{a}^\dagger) + E_J\left[1 - \cos(\hat{\varphi})\right] - \frac{E_J}{2}\hat{\varphi}^2, \tag{1.48}$$

where the driving term is equivalent to Equation 1.32. Because of the cosine term, this system evolves in a nontrivial manner.

Let us proceed by assuming a sinusoidal drive at ω_d. To calculate the effect of this drive, let us perform the following transformations (for details, see for instance [26]). First, we go into a rotating frame of the transmon ω. This is accomplished by the unitary operator [13],

$$\hat{U} = \exp(+\imath\omega t\hat{a}^\dagger\hat{a}), \tag{1.49}$$

which transforms our Hamiltonian as

$$\tilde{H} = \hat{U}\hat{H}\hat{U}^\dagger + \hat{U}\left[-\imath\frac{d}{dt}, \hat{U}\right]. \tag{1.50}$$

The resulting Hamiltonian is

$$\tilde{H} = \hat{H}_1 + \hat{U}\hat{H}_{nl}\hat{U}^\dagger \tag{1.51}$$

where $\hat{H}_1$ is our previous driven LC oscillator Hamiltonian (Eq. 1.33). Therefore, we have only to calculate the evolution of the nonlinear part of the Hamiltonian,

$$\tilde{H}_{nl} = e^{\imath\omega t\hat{a}^\dagger\hat{a}}\hat{H}_{nl}e^{-\imath\omega t\hat{a}^\dagger\hat{a}}. \tag{1.52}$$

We can rewrite the cosine term as

$$\cos\hat{\varphi} = \frac{1}{2}\left(e^{\imath\hat{\varphi}} + e^{-\imath\hat{\varphi}}\right). \tag{1.53}$$

Note that each of these exponential functions resembles a displacement operator, such

that

$$e^{\imath\hat{\varphi}} = e^{\imath\varphi_0(\hat{a}+\hat{a}^\dagger)}, \tag{1.54}$$

which has the same form as $\hat{D}(\imath\varphi_0)$ for a real number φ_0. Working with the exponential form simplifies calculations significantly since a displacement about any angle θ is still a displacement. More explicitly,

$$e^{i\theta\hat{a}^\dagger\hat{a}}\hat{D}(\alpha)e^{-i\theta\hat{a}^\dagger\hat{a}} = \hat{D}(\alpha e^{-i\theta}). \tag{1.55}$$

For $\theta = \omega t$, then, we see that our rotating frame has the effect of bringing the time dependence of the rotating frame into the cosine. Defining a rotating φ operator as

$$\tilde{\varphi} = \varphi_0\left(\tilde{a} + \tilde{a}^\dagger\right), \tag{1.56}$$

we then have

$$\tilde{H}_J = E_J\cos(\tilde{\varphi}). \tag{1.57}$$

Combining these terms, we are left with the rotating frame Hamiltonian

$$\tilde{H}(t) = \hbar\epsilon(t)\left(\tilde{a} + \tilde{a}^\dagger\right) + E_J\left[1 - \cos\left(\tilde{\varphi}\right)\right] - \frac{E_J}{2}\tilde{\varphi}^2, \tag{1.58}$$

We can use another unitary transformation to enter into the displaced frame of the drive [26]. This unitary has the form

$$\hat{U}_D = e^{-\xi(t)\hat{a}^\dagger + \xi^*(t)\hat{a}} \tag{1.59}$$

where $\xi(t)$ is a displacement amplitude. If the displaced mode has an energy decay rate κ, there is a clever choice of ξ such that the frame becomes stationary [27]. That condition is satisfied for the differential equation

$$\frac{d\xi}{dt} = -\left(\frac{\kappa}{2} + \imath\omega_0\right)\xi - \imath\epsilon(t) \tag{1.60}$$

If our drive is a simple, continuous wave (CW) drive at frequency ω_d, the solution to this differential equation is

$$\xi = -\frac{\imath\epsilon_0 e^{-\imath\omega_d t}}{\kappa_0 + \imath|\omega_d - \omega_0|}. \tag{1.61}$$

The squared-amplitude $|\xi|^2$ is effectively the number of drive photons. However, the amplitude ξ itself is quickly rotating.

By choosing our displaced frame as Equation 1.60 we are left with a displaced, rotating Hamiltonian that has a readily simplified form. Without any further approximations, the driven transmon atom Hamiltonian is

$$\tilde{H} = E_J \left[1 - \cos\left(\varphi_0(\tilde{a} + \tilde{a}^\dagger + \xi + \xi^*)\right)\right] - \frac{E_J \varphi_0^2}{2}(\tilde{a} + \tilde{a}^\dagger + \xi + \xi^*)^2 \tag{1.62}$$

To see the utility of the above expression, we again work in the small φ_0 limit. Now, we can expand Equation 1.62 in powers of φ and examine the allowed transitions of the circuit, as well as other 'real atom'-like effects. We expand the cosine using the Taylor series

$$\cos\vartheta = \sum_{k=0} \frac{(-1)^k}{(2k)!}\vartheta^{2k}. \tag{1.63}$$

When expanding the Hamiltonain (Eq. 1.62), the zeroth and second order terms will drop from our expression. We are left with

$$\tilde{H} = -E_J \sum_{k=2}^{\infty} \frac{(-1)^k \varphi_0^{2k}}{(2k)!} \left(\tilde{a} + \tilde{a}^\dagger + \xi + \xi^*\right)^{2k}. \tag{1.64}$$

To make further progress, we need make a few approximations. The first is that we will in practice only want to keep a finite number of terms. In fact, the lowest order (fourth order) already provides a rich set of physics to explore [26].

$$\tilde{H} \approx -\frac{E_J \varphi_0^4}{4!} \left(\tilde{a} + \tilde{a}^\dagger + \xi + \xi^*\right)^4 \tag{1.65}$$

The binomial theorem has useful generalizations for non-commuting operators, in particular Weyl operators $\left[\hat{A}, \hat{B}\right] = 1$, such as $\hat{a}$ and $\hat{a}^\dagger$. We can normal-order a polynomial of two Weyl operators [28] using

$$\left(\hat{A} + \hat{B}\right)^n = \sum_{m=0}^{n} \sum_{k}^{\mathrm{Min}[n, n-m]} C_{nmk} \hat{B}^{m-k} \hat{A}^{n-m-k} \tag{1.66}$$

where C_{nmk} is a combinatorial coefficient, given by

$$C_{nmk} = \frac{n!}{2^k k!(m-k)!(n-m-k)!}. \tag{1.67}$$

Because $\xi(t)$ is a complex number as opposed to an operator (representing the location of the displaced frame), ξ will commute with the other Hamiltonian terms. However,

by ignoring the noise terms associated with the drive, we are working in the limit of an infinitely stiff pump.

We make our second approximation before trying to solve the resulting dynamics. In the expansion, we will only keep energy conserving terms like $\tilde{a}^\dagger\tilde{a}$ or $\xi^*\xi$, since, for these terms, the quickly rotating parts (e.g. $e^{\imath\omega t}$) cancel, making these terms stationary. In the absence of drives ($\xi = 0$), our transmon Hamiltonian reduces to

$$\tilde{H} \approx -\frac{E_J\varphi_0^4}{4}\hat{a}^\dagger\hat{a}^\dagger\hat{a}\hat{a} \equiv -\frac{K}{2}\hat{a}^\dagger\hat{a}^\dagger\hat{a}\hat{a}. \tag{1.68}$$

This is a Kerr-type nonlinearity [29, 30], where the energy spectrum of the system depends quadratically on the transition level. If we look at the difference between neighboring Fock states, the splitting increases linearly as

$$E_{n+1} - E_n = -\frac{K}{2}\left(n(n+1) - n(n-1)\right) = -nK \tag{1.69}$$

Right away, we can see that if we have narrow enough frequency resolution, we may be able to resolve such an intrinsic energy splitting in spectroscopy. In later subsections, we will show that this intuition is correct but incomplete: spectroscopy on a Kerr-medium will turn out to be much richer than Equation 1.69 would suggest.

Another way to think of the Kerr nonlinearity is to consider a mean field frame about $\langle\hat{n}\rangle \approx \bar{n}$ [13]. We can reorder the nonlinearity as

$$\tilde{H} = \frac{K}{2}\left((\hat{a}^\dagger\hat{a})^2 - \hat{a}^\dagger\hat{a}\right) \tag{1.70}$$

Going into another rotating frame, at $\omega_{\bar{n}}$, will remove the second term on the right hand side. Another way to say that is that an oscillator with a Kerr-type nonlinearity has mean-field frequency that is proportional to the energy stored in the oscillator.

In the next subsections, we consider the effects of resonant and detuned drives $\omega_d \neq \omega_0$ on the transmon. We will see how our transmon atom can be excited or acquire an AC stark shift from drives.

1.3.4 Exciting a transmon atom

While the displaced frame treated us well when we were considering steady-states of the transmon, we abandon that transformation for the moment to consider a weak ($|\epsilon_0| \ll K$), resonant drive ($\omega_d = \omega_0$). We are particularly interested in how this drive affects the atom

to lowest level approximations. In the rotating frame of the ground state and drive, we have

$$\tilde{H} \approx -\frac{\hbar K}{2}\left(\hat{a}^\dagger\hat{a}^\dagger\hat{a}\hat{a}\right) + \hbar\epsilon_0\left(\hat{a}^\dagger + \hat{a}\right). \tag{1.71}$$

In the case of the linear LC oscillator, the drive term would displace the system until reaching equilibrium with the oscillator's decay rate. However, now higher states of the transmon are detuned from the drive, i.e.

$$|\epsilon_0| \ll |\Delta_{1\to 2}| = K, \tag{1.72}$$

where $\Delta_{1\to 2}$ is the detuning between the drive frequency and the $1 \to 2$ transition. Because of this detuning, the drive only dresses the higher states of the transmon virtually, giving them an AC Stark shift (as we will see in section 1.3.4). Our weak drive cannot actually excite these higher states at all.

The result is that transmon will undergo Rabi oscillations [31], where the population cycles between the ground and first excited state of the transmon. If we ignore the dressing effects of the higher-states, we can truncate our consideration to the lowest two levels of the transmon, treating it a qubit. Indeed, working with this reduced Hilbert space allows us to recover all of the simple Pauli matrix descriptions of qubits [31]. We can define Pauli operators

$$\hat{\sigma}_x \cong \hat{X} \tag{1.73a}$$

$$\hat{\sigma}_y \cong \hat{Y} \tag{1.73b}$$

$$\hat{\sigma}_z \cong 2\hat{a}^\dagger\hat{a}, \tag{1.73c}$$

where the congruency ($\cong$) is used to call attention to the crucial exception that the creation and annihilation operators are taken to only act on the lowest two states of the Hilbert space, i.e. $\hat{a}^\dagger|1\rangle \equiv 0$.

We can recast the truncated, resonantly driven Hamiltonian in a familiar form [31], as

$$\hat{H} = \frac{\hbar\epsilon_0}{2}\hat{\sigma}_x. \tag{1.74}$$

This effect is well described as a continuous rotation about the two-level system's Bloch sphere about the x-axis. The drive takes $|g\rangle$ to $|e\rangle$ in a time

$$T_{\text{Rabi}} = \frac{2\pi}{\epsilon_0} \tag{1.75}$$

Changing the phase of $|\epsilon|e^{\imath\theta}$ changes the Bloch-sphere angle that the procession will follow, e.g. along $\hat{\sigma}_y$ for $\theta = \pi/2$. Therefore, any point on the Bloch-sphere can be reached with this simple treatment. We will examine more of the consequences of this procession later (Section **??**). First though, there are a few more striking physical consequences that occur beyond the two-level atom description that are worth exploring.

Climbing the ladder

If we initialize the transmon in an excited Fock state, say the N^{th} Fock state, a choice of drive frequency can force Rabi oscillations between the $|N\rangle$ and $|N \pm 1\rangle$ states, allowing us to 'climb the ladder' of the transmon [32]. To see this, let us go into the rotating frame of given by

$$\omega_N = \omega_0 - \frac{K}{2}N(N-1). \tag{1.76}$$

If we consider just the nearest laying states we can write the undriven Hamiltonian as

$$\tilde{H}_0 = K\left[(N-1)\hat{\Pi}_{N-1} - N\hat{\Pi}_{N+1}\right], \tag{1.77}$$

where we have introduced the projection operator Π_N for simplicity, defined as

$$\hat{\Pi}_N = |N\rangle\langle N|. \tag{1.78}$$

Now, if we drive the transmon that detuned from our reference frame by $\Delta_d = \omega_d - \omega_N$, our driven Hamiltonian now has quickly oscillating terms. But, if we detune the drive by $\Delta_d = (N-1)K$ or $\Delta_d = -NK$ then we recover the two-level system description with the selected Fock state acting as $|g\rangle$ or $|e\rangle$. For example, taking $\Delta_d = -NK$ yields a similar expression to Equation 1.74 except now the Pauli matrix converts population between $|N\rangle$ and $|N+1\rangle$:

$$\tilde{\sigma}_x = |N\rangle\langle N+1| + |N+1\rangle\langle N| \tag{1.79}$$

It is clear by induction ($0 \Rightarrow 1$ and $N \Rightarrow N+1$) that all transmon levels can be reached in this fashion. In addition, because we can halt the Rabi oscillation at any point on a Bloch sphere, population can be spread across many levels of the transmon's Hilbert space, which can have arbitrary phase. The resulting state will be of the form

$$|\psi\rangle = \sum_n C_n|n\rangle. \tag{1.80}$$

However, for large states (spanning hundreds of excitations) with high symmetry, this process is cumbersome because each Fock state must be prepared individually. Later, we will see how another nonlinearity can provide some amount of parallelization to our toolbox (Section ??).

AC Stark effect in a transmon atom

The AC Stark effect describes the response of an atom to a rapidly rotating external field [33]. In this process, the atom acquires a dressing due to the detuned drive ($\Delta = \omega_d - \omega_0$), causing the spectrum of the atom to change. Dressed-state splitting has deep connections to nonlinearity. Recall that the 'spectrum' of the harmonic LC oscillator was unaffected by any drive. Observing that a circuit exhibits the AC Stark effect, as in Schuster et al. [34], is evidence that the system interacts with light in a highly nontrivial manner.

Consider Equation 1.65 with a very detuned drive ($\Delta \gg K$), such that the only terms valid in the Rotating Wave Approximation (RWA) [31] are $\hat{a}^\dagger\hat{a}$ and $\xi^*\xi$. We use the expansion coefficients (Eq. 1.67) to write down that

$$\tilde{H}_{\text{stark}}(t) \approx -\frac{K}{2}\left(\hat{a}^\dagger\hat{a}^\dagger\hat{a}\hat{a} + \hat{a}^\dagger\hat{a}|\xi(t)|^2\right). \tag{1.81}$$

Thus, the transmon has acquired a new dressed frequency that is proportional to the power contained in the AC drive. The new frequency is detuned by

$$\Delta_{\text{stark}}(t) = -\frac{K}{2}|\xi(t)|^2 \tag{1.82}$$

For a CW drive, we can use Equation 1.61 to write

$$\Delta_{\text{stark}} = -\frac{\bar{K}}{2} \times \left(\frac{\epsilon_0^2}{\kappa_0^2 + (\omega_d - \omega_0)^2}\right). \tag{1.83}$$

Essentially, even virtual photons (i.e. $|\xi(t)|^2 \gg 0$ but $|\hat{a}^\dagger\hat{a}| \approx 0$) can load the Kerr nonlinearity.

AC Stark effect in a two-level atom

In the weak driving ($\epsilon \ll K$), small detuning ($\Delta \ll K$) limit, wherein the transmon is well-approximated as a two level system, we can solve for the AC Stark effect as commonly

done for qubits [31]. The Hamiltonian is thus

$$\hat{H} = \frac{\hbar\Delta}{2}\sigma_z - \frac{\hbar\epsilon_0}{2}\sigma_x \tag{1.84}$$

The new, dressed eigenstates have energies

$$E_\pm = -\frac{\hbar\epsilon_0}{2} \pm \frac{\hbar}{2}\sqrt{\epsilon_0^2 + \Delta^2}. \tag{1.85}$$

For $\Delta \gg \epsilon_0$ we have shifted the ground state energy by

$$\delta E_- \approx \frac{\hbar\epsilon_0^2}{4\Delta^2} + \mathcal{O}\left(\frac{\epsilon_0}{\Delta}\right)^4 \tag{1.86}$$

1.3.5 Selection rules and multi-photon transitions

It turns out that we can take short cuts on our way up the ladder too. At higher order approximations, multi-photon transitions become allowed at certain drive frequencies [21]. For fourth-order approximations to our transmon atom, we will show explicitly that two-photon transitions between second-nearest neighbors is allowed. We then give a recipe for extending these ideas to arbitrary transitions, allowing us to define selection rules for our artifical atom.

For a second-order transition, we need terms in the Hamiltonian which connect second-nearest neighbors like

$$\hat{H}_{\text{two-photon}} = \hbar\epsilon_0\left((\hat{a}^\dagger)^2 + \hat{a}^2\right). \tag{1.87}$$

To see how these can come about, we start from the rotating, displaced picture at fourth-order (Eq. 1.65). There will always be terms in the binomial expansion of this Hamiltonain which have the form

$$\hat{H}_2 \propto \left(\xi^2(\hat{a}^\dagger)^2 + (\xi^*)^2\hat{a}^2\right). \tag{1.88}$$

These terms are usually thrown out by the RWA. However, consider a drive at a frequency halfway between a given Fock state and its second-nearest neighbor, $\omega_d = \frac{1}{2}(\omega_{N+2} + \omega_N) = \frac{1}{2}(\omega_N - N^2K)$. Then, two-photon terms like the above rotate at

$$\xi^2(t)(\tilde{a}^\dagger)^2 = \xi^2(\hat{a}^2)e^{2\imath(\omega_d - \omega_N)t} = \xi^2(\hat{a}^2)e^{-\imath N^2 K t} \tag{1.89}$$

But, we see that since the $|N+2\rangle$ state has an energy difference with the $|N\rangle$ state of $\delta E = -N^2K$, that time dependence is actually the correct rotating frame for the

$N \to N+2$ transition! Importantly, the selection rule is proportional to $|\xi|^2$, meaning that the Rabi rate now given by the square of the drive strength, now a function of ϵ_0^2.

In practice, this is a useful way to characterize the anharmonicity of a transmon circuit in spectroscopy [21]. At sufficiently large drive strengths (enough that ϵ_0^2 can saturate the transition), the detuning between a two-photon transition and a single-photon transition gives us value of K directly ($\Delta f = K/2$). Furthermore, this type of transition is easily distinguished from the single-photon transition because the $|\epsilon_0|^2$ dependence reduces line-broadening. Thus, the higher-order terms tend to be more narrow in spectroscopy, as shown in Section **??**.

Sixth order expansion will give terms that are of the form $\xi^3(\hat{a}^3)$ and that a drive at the appropriately chosen frequency can drive this term proportional to $|\epsilon_0|^3$, and these transitions can be observed as well [35]. Indeed, all transitions of the transmon atom would be accessible by continuing this pattern. However, an $\mathcal{O}^{th}$ order transition is exponentially hard to drive. Therefore, at some high order, we will break the approximation that $\epsilon_0 \ll K$. Hence, these processes will no longer be selective. We will essentially start driving many transitions at once, instead of driving single Rabi-like oscillations in Fock-space.

1.4 Coupling quantum circuits

Adding more degrees of freedom to our circuit, in the form of additional components, can enable new functionality. For instance, circuits with multiple superconducting qubits can be used to execute quantum algorithms [36] or quantum error correction [37–40]. Moreover, circuits with dissimilar types of components [41] can be useful for applications such as quantum memory [42–44] or quantum communication [45].

One particularly important class of coupled circuits is a superconducting qubit coupled to a linear resonator. This is a scheme known as circuit QED (cQED) [46, 47] for its close analogues with Cavity QED (CQED) [13]. A cQED-type architecture protects superconducting qubits from spontaneous emission [48], allows for multi-qubit gates [49, 50], and enables high fidelity, QND measurements of qubit states [51, 52]. In this section, we describe the theory of coupled transmon-resonator circuits, closely following the approach used in Section 1.3.1 to describe a single transmon.

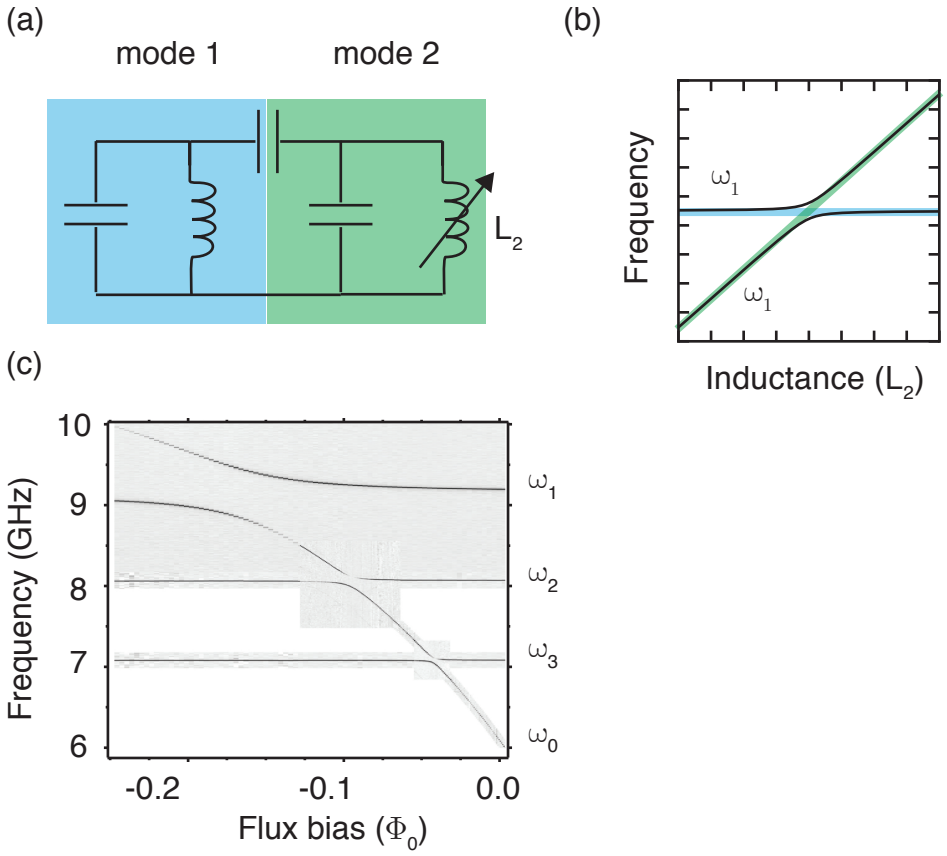

Figure 1.7: Classical dressing of a linear circuit. **(a)** Two parallel LC resonators are joined by a capacitor to form a simple coupled-circuit. Because of their interaction, neither mode preserves its independence. This effect can revealed by sweeping any circuit element, e.g. mode two's inductor L_2, and observing the new eigenmodes of the system. **(b)** The linear circuit can be exactly diagonalized. The spectrum is shown as a function of L_2, with shading representing the behavior of the two modes in the absence of coupling. The resulting eigenmodes are $\omega_\pm = (\omega_1 + \omega_2 \pm \sqrt{g^2 + \Delta^2})/2$, where Δ is the detuning and g is the coupling strength. Near resonance ($\Delta = 0$), a level repulsion of $\omega_+ - \omega_- = 2g$ is caused by the interaction. The techniques in this chapter that diagonalize linear parts of more complicated systems capture effects such as this mode-splitting. The splitting between these two LC modes is a classical effect and can be observed with standard circuit elements on printed circuit boards. **(c)** Spectroscopy data of the realization of avoided crossings in cQED. A flux-tunable transmon qubit is tuned through resonance of several other modes. The size of the avoided crossings is a classical parameter, although the evolution of the system at any of these bias points is highly quantum. (Figure used with permission from [37]. See **??**.)

1.4.1 Black Box Quantization for many modes

The techniques for treating the Josephson nonlinearity as a perturbation can be extended to systems with many coupled elements [3]. Before (Section 1.3.1), we proceeded by diagonalizing the linear Hamiltonian, then introducing a term $\hat{H}_{nl}$ to account for a nonlinear inductance of the junction. For coupled circuits, we must solve a system of many hybridized LC modes. However, the result will always be expressible as some number of resonant modes [53], although the frequencies and characteristic impedances for an LC resonance may be altered by the coupling. The linear Hamiltonian, after this diagonalization, can therefore be written as

$$\hat{H}_{tot} = \hbar \sum_n \tilde{\omega}_n \hat{\mathcal{A}}_n^\dagger \hat{\mathcal{A}}_n \tag{1.90}$$

where $\hat{\mathcal{A}}_n$ represents the annihilation operator of the n-th, re-diagonalized mode. Because these new eigenmodes are the same as their classical counterparts (Fig. 1.7), classical circuit analysis is sufficient to solve this part of the system.

All we need now to treat the effects of our Josephson junction is the dressing of these modes as seen at the 'port' of the junction. Essentially, each mode will contribute some amount of flux toward the junction, as

$$\hat{\Phi} = \sum_n \Phi_{\mathrm{ZPF}}^n \left(\hat{\mathcal{A}}_n^\dagger + \hat{\mathcal{A}}_n \right) \tag{1.91}$$

Luckily, we already know how to find the required Φ_{ZPF}^n parameters too!

We saw earlier that the magnitude of the zero-point fluctuations was simply related to the effective impedance of the circuit by Equation 1.10a. We now see that the relevant characteristic impedance is the mode's impedance as seen by the junction. To find these zero-point fluctuation values, we simply need to determine impedance of each mode.

Imagine that we had an impedance-probe at the junction looking out, which could measure across a wide-range of frequencies. At each normal mode of the circuit, our admittance would cross zero (giving us $\tilde{\omega}_n$). Further, the slope of the admittance trace at that zero-crossing is related to the mode's effective characteristic impedance [3], as

$$\left(\frac{dY}{d\omega} \right) \Big|_{\omega=\tilde{\omega}_n} = \frac{2j}{\tilde{\omega}_n Z_{\mathrm{eff}}} \equiv Y_n' \tag{1.92}$$

By rearranging Equation 1.92, we find a simple way relate the effective impedance that sets the scale of the zero-point fluctuations to a measurable, at least in theory, circuit

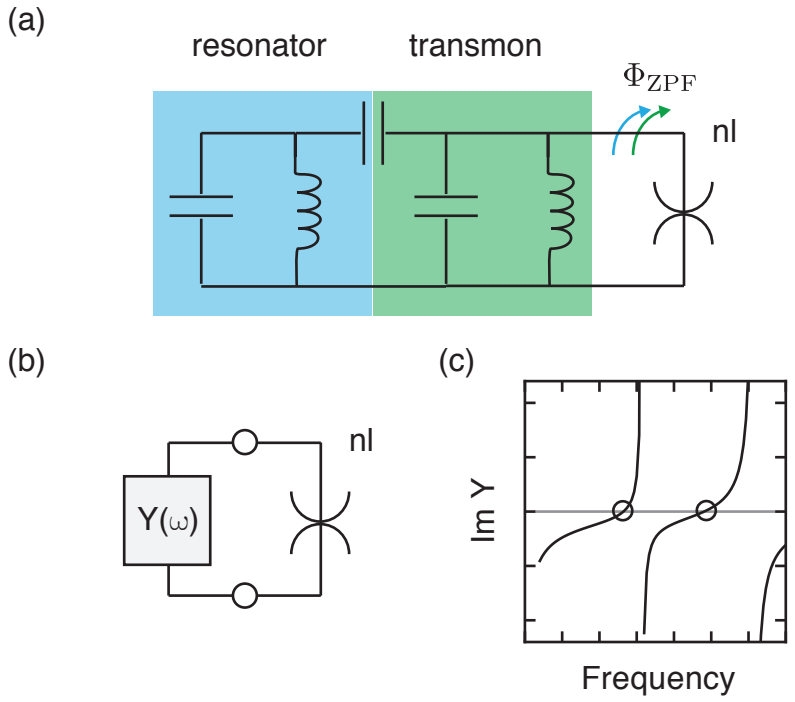

Figure 1.8: Black box quantization of many modes. (a) The most basic circuit QED schematic is a mostly-linear LC oscillator (resonator) coupled to a strongly nonlinear LC oscillator (transmon). Both acquire their nonlinearity from a single Josephson element, which also provides the cross mode-mode nonlinearity (such as cross-Kerr term χ) to the system. **(b)** To simplify the quantum mechanical treatment of the coupled system, first the classical circuit is diagonalized and lumped into a 'black box' admittance term $Y(\omega)$. **(c)** The characteristic impedance of each resonant mode in the black box, as viewed from the junction, sets the participation of that mode in the junction's nonlinearity. That impedance can be predicted from studying the classical circuit model of the system. The problem reduces to finding the zero-crossings of the imaginary part of the admittance and the slope of the function there (circles).

parameter. Now, the magnitude of the zero-point fluctuations are given by

$$\Phi^n_{\mathrm{ZPF}} = \frac{\Phi_0}{\sqrt{2\pi R_Q \tilde{\omega}_n Y'_n}}, \tag{1.93}$$

where R_Q is the resistance quantum. Because Y'_n is a classical, linear circuit parameter, traditional circuit simulators are also able predict Φ^n_{ZPF} natively, even for complex circuits [3].

Our total Hamiltonian now reads

$$\hat{H} = \hbar \sum_n \tilde{\omega}_n \hat{\mathcal{A}}^\dagger_n \hat{\mathcal{A}}_n + \hat{H}_{nl} \tag{1.94}$$

where $\hat{H}_{nl}$ is defined equivalently to before (Eq. 1.45), except we replace the simple flux operator by our new expression for total flux across the junction (Eq. 1.91) [3], giving the full Hamiltonian as

$$\hat{H}_{nl} = E_J \left[1 - \cos\left(\sum_n \varphi_n \left(\hat{\mathcal{A}}^\dagger_n + \hat{\mathcal{A}}_n \right) \right) \right] - \frac{E_J}{2} \left[\sum_n \varphi_n \left(\hat{\mathcal{A}}^\dagger_n + \hat{\mathcal{A}}_n \right) \right]^2 \tag{1.95}$$

where again, we will find it simpler to work in a unitless parameter $\varphi_n \equiv \Phi^n_{\mathrm{ZPF}}/\Phi_0$. Indeed, the sum over all fluxes shows up as the operator $\hat{\varphi}_{\mathrm{tot}}$, including for the quadratic term on the right hand side.

The real utility of this total Hamiltonian becomes clear when we consider the fact that distinct modes commute: $\left[\hat{\mathcal{A}}_n, \hat{\mathcal{A}}_m\right] = \delta_{n,m}$. Therefore, our frame transformations from before can be done in parallel on this potentially massive Hamiltonian right away. Going into the co-rotating frame, such that $\tilde{\mathcal{A}}_n = \hat{\mathcal{A}}_n e^{\imath \tilde{\omega}_n}$, allows us to expand the total Hamiltonian like before.

For simplicity, let us treat in some detail the simple case of two modes, truncated at the fourth order. We can write the truncated Hamiltonian (similar to Eq. 1.65) as

$$\tilde{H} \approx \frac{\hbar E_J}{24} \left[\varphi_a \left(\tilde{a}^\dagger + \tilde{a} \right)^4 + \varphi_b \left(\tilde{b}^\dagger + \tilde{b} \right) \right]^4 \tag{1.96}$$

We use the RWA to find the dominant terms of this Hamiltonian [13]. In particular, because our modes are detuned, we can discard terms like $\tilde{a}^\dagger \tilde{b}$ in the expansion of the quartic Hamiltonian. Collecting terms like $\tilde{a}^\dagger \tilde{a}$ and $\tilde{b}^\dagger \tilde{b}$, we see that each mode will acquire

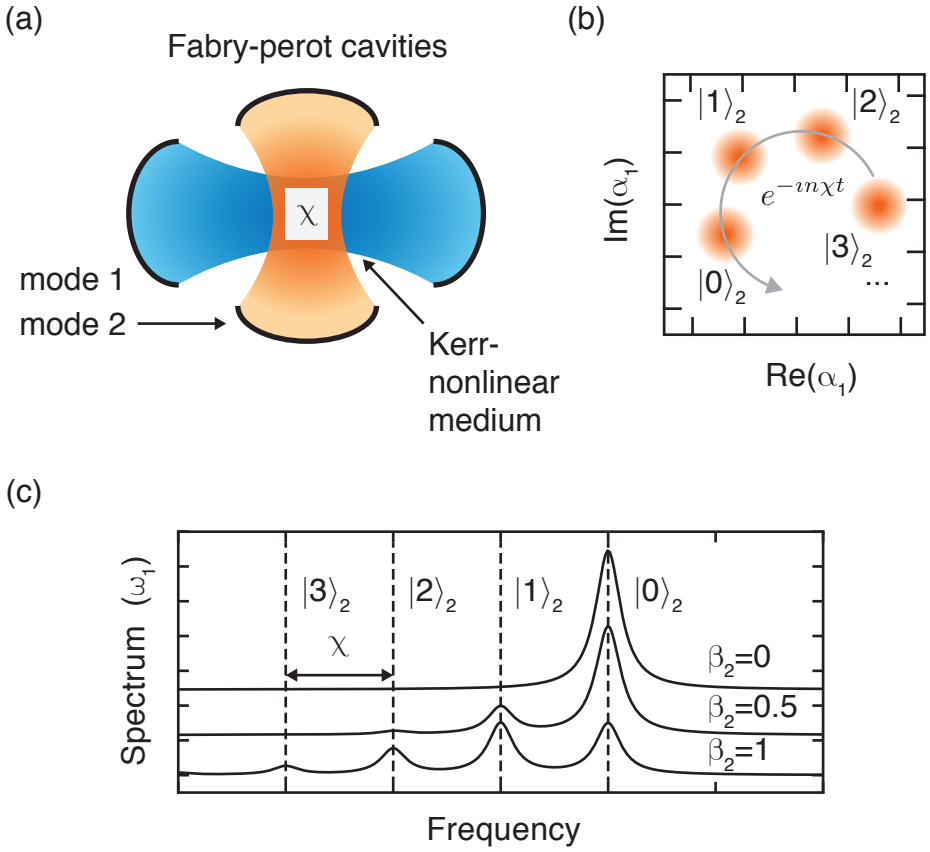

Figure 1.9: Cross-Kerr nonlinear effects. (a) Two prototypical oscillators, modes one and two (shown as Fabry Perot-type resonators), store energy in a Kerr nonlinear medium. In that nonlinear medium, the phase velocity of resonant light depends on the total energy stored, leading to an effective length for the resonators which is dependent on the energy stored in the other. A strongly nonlinear version of this system is realized in cQED architectures with remarkable consequences. **(b)** If mode two is in a superposition of several Fock states, for instance as a coherent state $|\beta\rangle_2$, any state in mode one, shown as a single Gaussian state, acquires a differential phase for each Fock state $|m\rangle_2$ at a rate χ, where χ is the strength of the cross-Kerr nonlinearity. **(c)** With strong nonlinearity ($\chi \gg \kappa$, where κ is the linewidth of the modes), the system enters the number-split regime of cross-Kerr interaction. Each energy eigenstate of mode two $|m\rangle_2$ is associated with its own transition frequency in mode one. Shown are frequency spectra of mode one for three different coherent states in mode two.

a Kerr term proportional to

$$K_k = \frac{E_J \varphi_k^4}{4} \tag{1.97}$$

This is a little strange. Our circuit under consideration began as a transmon sub-circuit coupled to many LC oscillators, but somehow, we ended up with just a bunch of transmons! In retrospect, this might not be too surprising since a transmon, in our treatment, has been a nonlinearly-shunted LC oscillator. Surely then, by introducing the same nonlinearity to the other LC oscillators, they might be expected to dress with the Josephson effect in a similar manner.

At fourth order, we acquire a new type of Hamiltonian term as well that has interesting consequences for our circuit. We now find terms in the expansion that are a cross-Kerr type nonlinearity [54], as

$$\tilde{H}_{\text{int}} = -E_J \varphi_a^2 \varphi_b^2 \hat{a}^\dagger \hat{a} \hat{b}^\dagger \hat{b}. \tag{1.98}$$

We define the cross-Kerr interaction strength as $\chi_{ab} \equiv E_J \varphi_a^2 \varphi_b^2$. Note that χ is related to the geometric mean of the two Kerr terms as

$$\chi_{ab} = 2\sqrt{K_a K_b}. \tag{1.99}$$

This makes intuitive sense since this nonlinear interaction is set by how hybridized each mode is to the single Josephson junction in the problem. That same hybridization also sets K_n.

For two modes with a large detuning, χ_{ab} is the dominant coupling term. This regime is known as the dispersive regime of cQED [54], a Hamiltonian that has also obtained with CQED [13]. Now, if mode a is excited, for example in the Fock state $|1\rangle_a$, our dispersive Hamiltonian indicates that the frequency of mode b will shift downward by exactly χ, since $\langle \hat{a}^\dagger \hat{a} \rangle = 1$ for Equation 1.98. A more interesting behavior is achieved whenever one of the modes is in a superposition of Fock states. Then, an entangling interaction occurs [13], whereby a superposition of Fock states in one mode forces the other mode to be in a conditional superposition of many frequencies, as we will discuss in detail in Chapter **??**. In the next section, we show how this conditional frequency shift can be used to devise a QND measurement of the qubit state.

1.5 Detecting the state of a transmon

It might be interesting to probe a transmon directly with a Vector Network Analyzer (VNA), for instance, measuring the atom in reflection, similar to the scheme of Hoi et al. [55]. In this case, when the VNA (at weak probe powers) sweeps through a transition frequency of an occupied level of our transmon, a single probe photon (at most) will be exchanged with the transmon. Detecting a missing photon (absorption) or an extra photon (emission) would inform us of the former state of the transmon. However, practically this is a demanding requirement. Additionally, the real impedance of the VNA would introduce unnecessary dissipation to the transmon, as we will discuss later in Section **??**.

Instead, we will couple our simple transmon circuit to a filter element, an ancillary LC oscillator [46, 47], and probe the response of the oscillator to infer information about the state of the transmon [2, 56]. To detect the state of mode a, we need to determine mode b's frequency with sufficient precision to determine whether it is ω_b or $\omega_b - \chi$. There are some nice properties of this proposal. First, if we can drive mode b with many photons, our frequency detector does not need to be sensitive to fluorescence-like signal levels as considered before. Also, this detection can be QND to good approximation [51, 52]. This is opposed to schemes which rely on absorption or fluorescence, which detect a change of state. Finally, if the readout mode is more strongly coupled to the detection apparatus, it will filter real impedance of the detector from the transmon atom, extending the possible lifetimes in the transmon mode [48].

Now, however, our readout mode has acquired some transmon-like behavior as shown in the previous section. However, for a carefully designed circuit, we can largely ignore these effects, and pretend that our filter retains its linearity. This is a reasonable approximation for the readout mode whenever

$$K_b |\langle \hat{b}^\dagger \hat{b} \rangle|^2 \ll 1/T_{\text{exp}} \tag{1.100}$$

where T_{exp} is the timescale for the experiment. Essentially, for a weak nonlinearity, the number-state dependent phase accumulation by the Kerr effect may take more time to acquire than we are sensitive to.

To use the conditional frequency shift of the readout mode ($\delta\omega = \chi$) as a detection mechanism, sufficient frequency precision is required. Therefore, the measurement time

will be on the order of $T_{\text{exp}} \approx 1/\chi$. By Equation 1.100, we then require that

$$\chi_{ab} \gg K_b \langle \hat{b}^\dagger \hat{b} \rangle. \tag{1.101}$$

Therefore, we must design circuits that have a large χ_{ab}/K_b ratio. Using Equation 1.99, we find that these requirements can be distilled to working with a transmon having high anharmonicity, such that

$$\mathrm{K}_a \gg K_b |\langle \hat{b}^\dagger \hat{b} \rangle|^2. \tag{1.102}$$

Essentially, the above constraint is the extent to which we can assign the label 'transmon' to one mode and 'resonator' to the other. In practice, this inequality is easily satisfied because usually only the transmon mode is galvanically connected to the junction. For instance, we will study a sample in detail in Chapter **??** that fulfills this requirement up to $\langle \hat{b}^\dagger \hat{b} \rangle \approx 500$.

To show how the simplest readout schemes operate, consider our coupled Hamiltonian, with the transmon truncated at its lowest two levels (Eq. 1.73), and ignoring the resonator's nonlinearity [46]. In the interaction picture, the Hamiltonian is given by

$$\tilde{H}_{\text{disp}} = \frac{\chi_{ab}}{2} \hat{b}^\dagger \hat{b} \hat{\sigma}_z. \tag{1.103}$$

This expression is equivalent to the dispersive limit of the Jaynes-Cummings model for CQED [13], albeit derived with a different set of systems, assumptions and approximations.

A typical technique for measuring the frequency of a resonator is to measure the reflection coefficient of signals from the device [2, 56]. That coefficient is given by

$$r = \frac{\Delta_b - \imath\kappa/2}{\Delta_b + \imath\kappa/2} \tag{1.104}$$

where Δ_b is the detuning between the probe and the resonator. For a probe tone tuned halfway between the response of mode b to the transmon ($\omega_d = \omega_b - \chi/2$), r can be rewritten to account for the state-dependent shift [2] as

$$r = \frac{\chi \hat{\sigma}_z - \imath\kappa/2}{\chi \hat{\sigma}_z + \imath\kappa/2}. \tag{1.105}$$

If we define a the angle $\theta = \kappa/\chi$ we can simplify the reflection as a rotation in the IQ plane as

$$r = e^{-\imath\theta\hat{\sigma}_z}. \tag{1.106}$$

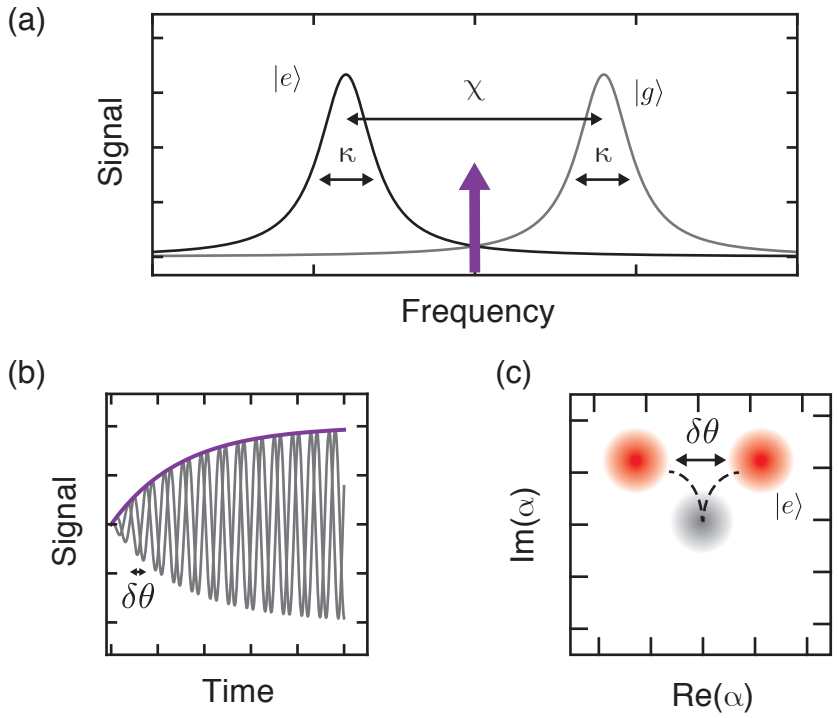

Figure 1.10: Reading out the state of a transmon. (a) The frequency of the readout resonator depends strongly on the state of the transmon qubit. The frequency shift χ can be much greater than the linewidth of the mode κ. To probe the state of the transmon, a common technique is to drive halfway between these two frequencies (purple arrow). Then, the state of the transmon is encoded in the phase of the outgoing signal. **(b)** A readout pulse builds up energy in the resonator that is leaked out to the measurement chain. For the readout probe frequency shown in (a), the two states of the transmon yield identical ring-up type envelopes. **c)** The amplitude and phase of these signals are digitized, via techniques described in a later chapter, and the measurement results are histogrammed. The relative counts between the two distributions gives the probability the qubit was detected in the ground or excited state (P_g and P_e).

For a coherent input state, in the absence of the resonator's Kerr nonlinearity, this phase angle is independent of the displacement size [2]. Therefore, phase contrast, our measurement signal, will increase with larger displacements. We can quantify the information contained in the reflected signal as the orthogonality of the resultant coherent states. If the two states of the transmon ($|0\rangle_a, |1\rangle_a$, or equivalently $|g\rangle, |e\rangle$) are mapped onto a phase difference θ, the coherent states can be detected in unique states to the extent that

$$\langle \alpha e^{+\imath\theta} | \alpha e^{-\imath\theta} \rangle = 0 \tag{1.107}$$

We give the practical details of this detection scheme later in Section ??.

1.5.1 Selection rules for many-wave mixing

We conclude our study of the simplest coupled-oscillator Josephson circuits with some striking effects that can be observed by stimulating otherwise negligible processes in the circuit with pumps.

We rely on the commutativity of our different modes in order to go into a co-rotating, co-displaced frame [26], such that all modes can be driven by some field, transforming our operators as

$$\tilde{\mathcal{A}}_n \rightarrow \tilde{\mathcal{A}}_n + \xi_n. \tag{1.108}$$

Our total Hamiltonian recovers a generalized form of Equation 1.62. A remarkable set of interactions can be driven between the elements of our many-transmon artificial molecule.

If we take the simplest experiment, driving a single mode off resonantly, the χ interaction at fourth order approximation ends up every mode an AC Stark shift [26]. Driving the n-th mode shifts the m-th mode by an amount

$$\Delta_m = -\chi_{nm} |\xi_n|^2. \tag{1.109}$$

Also, similar the multi-photon transitions of a single transmon, strong pumps can drive multi-photon processes in the coupled circuit [26]. For example, a pump on mode n at a frequency $\omega_d = \frac{1}{2}(\omega_m - \omega_n)$ would make stationary any terms in the Hamiltonian of the form

$$\hat{H}_{swap} = -\chi_{nm} \left[\xi^2 \tilde{\mathcal{A}}_n{}^\dagger \tilde{\mathcal{A}}_m + (\xi^*)^2 \tilde{\mathcal{A}}_n \tilde{\mathcal{A}}_m{}^\dagger \right] \tag{1.110}$$

We see that this Hamiltonian term can be used to swap single photons between modes, such as the transmon and resonator, by exchanging energy with two probe photons (four-wave

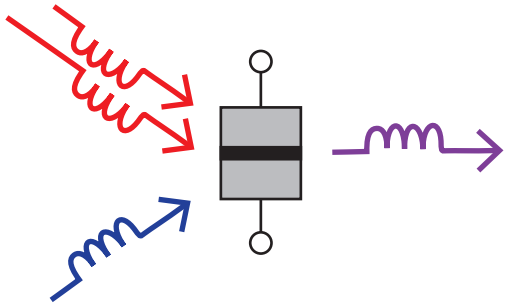

Figure 1.11: Josephson junction as a scattering site. Many Hamiltonian terms are discarded by energy conservation considerations during the polynomial treatment of a Josephson junction's cosine potential. However, in the presence of drives, these otherwise neglected terms can dominant the evolution of the system. Pumping a single junction at multiple frequencies can lead to a versatile set of mode conversions via many-wave mixing.

mixing). For a cold resonator with fast decay constant, this technique can be used for to reset another mode [26]. Or, driven between two coherent modes, this pump can be used for SWAP-based quantum logic [57]. Interestingly, these SWAP interactions typically require resonant operation [57] (and thus frequency tunability), which can complicate circuit implementations. Here, we get that physics 'for free' from the quartic term of our cosine expansion.

As another example, take the pump frequency $\omega_d = (2\omega_m - \omega_n)$. Energy-conserving terms now include

$$\hat{H}_{swap} = -\chi_{nm}\left[\xi\left(\tilde{\mathcal{A}}_n^{\dagger}\right)^2\tilde{\mathcal{A}}_m + \xi^*\left(\tilde{\mathcal{A}}_n\right)^2\tilde{\mathcal{A}}_m^{\dagger}\right] \tag{1.111}$$

Just by changing the frequency of the pump, we have altered the four wave mixing such that now one photon from mode m is converted to two photons in mode n and vice-versa, by exchanging energy with a single pump photon. This parametric process was used in Leghtas et al. [26] to drive an oscillator directly to a cat state.

There is an infinite number of interesting processes we can stimulate with many-wave mixing [29]. The recipe is simple enough to be extended to even higher order terms beyond quartic. These experiments will push the cosine expansion in new ways. Single Josephson junction circuits seem to be an endless playing field for fundamental quantum optics.

Before diving into the physical implementation of these systems, the next chapter explores the consequences of quantum information in resonators. Future chapters will

discuss the specifics of transmon-resonator design Chapter ?? as well as techniques for their fabrication and measurement Chapter ??. Then we will combine these ideas to describe a novel type of quantum memory that has state-of-the-art coherence for cQED, in Chapter ??.

Bibliography

1. M. H. Devoret, "Quantum fluctuations in electrical circuits," in *Mesoscopic Quantum Physics: Lecture Notes of the Les Houches Summer School: Volume 61, July 1994*, E. Akkermans, G. Montambaux, J. L. Pichard, and J. Zinn-Justin, eds., Lecture Notes of the Les Houches Summer School: Volume 61, July 1994. Elsevier Science Ltd, Feb., 1996. Cited on pages 1, 3, 4, 6, 12 & 14.

2. S. M. Girvin, "Superconducting qubits and circuits: Artificial atoms coupled to microwave photons," in *Quantum Machines: Measurement and Control of Engineered Quantum Systems: Lecture Notes of the Les Houches Summer School: Volume 96, July 2011*, M. Devoret, B. Huard, R. Schoelkopf, and L. F. Cugliandolo, eds., Lecture Notes of the Les Houches Summer School: Volume 96, July 2011. OUP Oxford, June, 2014. Cited on pages 1, 3, 4, 5, 9, 32, 33 & 35.

3. S. E. Nigg, H. Paik, B. Vlastakis, G. Kirchmair, S. Shankar, L. Frunzio, M. H. Devoret, R. J. Schoelkopf, and S. M. Girvin, "Black-box superconducting circuit quantization," *Phys. Rev. Lett.* **108**, 240502 (2012). Cited on pages 1, 14, 15, 16, 27 & 29.

4. J. Clarke and F. K. Wilhelm, "Superconducting quantum bits," *Nature* **453**, 1031–1042 (2008). Cited on pages 2 & 15.

5. M. H. Devoret and R. J. Schoelkopf, "Superconducting circuits for quantum information: An outlook," *Science* **339**, 1169–1174 (2013), http://www.sciencemag.org/content/339/6124/1169.full.pdf. Cited on pages 2 & 15.

6. C. Kittel, *Introduction to Solid State Physics*. Wiley, 2004. https://books.google.com/books?id=kym4QgAACAAJ. Cited on page 2.

7. M. Tinkham, *Introduction to Superconductivity*. Dover Books on Physics Series. Dover Publications, 1996. Cited on pages 2 & 12.

8. V. B. Braginsky, Y. I. Vorontsov, and K. S. Thorne, "Quantum nondemolition measurements," *Science* **209**, 547–557 (1980), http://www.sciencemag.org/content/209/4456/547.full.pdf. Cited on page 5.

9. M. Aspelmeyer, T. J. Kippenberg, and F. Marquardt, "Cavity optomechanics," *Rev. Mod. Phys.* **86**, 1391–1452 (2014). Cited on page 6.

10. R. J. Glauber, *Quantum Theory of Optical Coherence: Selected Papers and Lectures*. Wiley, 2007. Cited on pages 6, 7 & 10.

11. R. J. Glauber, "Coherent and incoherent states of the radiation field," *Phys. Rev.* **131**, 2766–2788 (1963). Cited on pages 7, 9 & 10.

12. W. M. Itano, C. R. Monroe, D. M. Meekhof, D. Leibfried, B. E. King, and D. J. Wineland, "Quantum harmonic oscillator state synthesis and analysis," in *Atom Optics*, M. G. Prentiss and W. D. Phillips, eds., vol. 2995 of *Society of Photo-Optical Instrumentation Engineers (SPIE) Conference Series*, pp. 43–55. May, 1997. quant-ph/9702038. Cited on pages 9 & 10.

13. S. Haroche and J. M. Raimond, *Exploring the Quantum: Atoms, Cavities, and Photons*. Oxford Univ. Press, Oxford, UK, 2006. Cited on pages 10, 17, 20, 25, 29, 31 & 33.

14. B. D. Josephson, "The discovery of tunnelling supercurrents," *Rev. Mod. Phys.* **46**, 251–254 (1974). Cited on page 11.

15. B. D. Josephson, "Possible new effects in superconductive tunnelling," *Physics Letters* **1**, 251–253 (1962). Cited on page 12.

16. Y. Makhlin, G. Schön, and A. Shnirman, "Quantum-state engineering with josephson-junction devices," *Rev. Mod. Phys.* **73**, 357–400 (2001). Cited on page 12.

17. J. Q. You and F. Nori, "Atomic physics and quantum optics using superconducting circuits," *Nature* **474**, 589–597 (2011). Cited on page 14.

18. N. Bergeal, F. Schackert, M. Metcalfe, R. Vijay, V. E. Manucharyan, L. Frunzio, D. E. Prober, R. J. Schoelkopf, S. M. Girvin, and M. H. Devoret, "Phase-preserving amplification near the quantum limit with a Josephson ring modulator," *Nature* **465**, 64–68 (2010). Cited on page 15.

19. B. Abdo, K. Sliwa, F. Schackert, N. Bergeal, M. Hatridge, L. Frunzio, A. D. Stone, and M. Devoret, "Full coherent frequency conversion between two propagating microwave modes," *Phys. Rev. Lett.* **110**, 173902 (2013). Cited on page 15.

20. K. M. Sliwa, M. Hatridge, A. Narla, S. Shankar, L. Frunzio, R. J. Schoelkopf, and M. H. Devoret, "The reconfigurable Josephson circulator/directional amplifier," *ArXiv e-prints* (2015), 1503.00209 [quant-ph]. Cited on page 15.

21. A. Houck, J. Koch, M. Devoret, S. Girvin, and R. Schoelkopf, "Life after charge noise: recent results with transmon qubits," *Quantum Information Processing* **8**, 105–115 (2009). Cited on pages 15, 24 & 25.

22. J. Koch, T. M. Yu, J. Gambetta, A. A. Houck, D. I. Schuster, J. Majer, A. Blais, M. H. Devoret, S. M. Girvin, and R. J. Schoelkopf, "Charge-insensitive qubit design derived from the cooper pair box," *Phys. Rev. A* **76**, 042319 (2007). Cited on pages 15 & 16.

23. J. A. Schreier, A. A. Houck, J. Koch, D. I. Schuster, B. R. Johnson, J. M. Chow, J. M. Gambetta, J. Majer, L. Frunzio, M. H. Devoret, S. M. Girvin, and R. J. Schoelkopf, "Suppressing charge noise decoherence in superconducting charge qubits," *Phys. Rev. B* **77**, 180502 (2008). Cited on page 15.

24. L. Sun, L. DiCarlo, M. D. Reed, G. Catelani, L. S. Bishop, D. I. Schuster, B. R. Johnson, G. A. Yang, L. Frunzio, L. Glazman, M. H. Devoret, and R. J. Schoelkopf, "Measurements of Quasiparticle Tunneling Dynamics in a Band-Gap-Engineered Transmon Qubit," *Physical Review Letters* **108**, 230509 (2012), 1112.2621 [cond-mat.mes-hall]. Cited on page 16.

25. Y. Nakamura, Y. A. Pashkin, and J. S. Tsai, "Coherent control of macroscopic quantum states in a single-Cooper-pair box," *Nature* **398**, 786–788 (1999), cond-mat/9904003. Cited on page 17.

26. Z. Leghtas, S. Touzard, I. M. Pop, A. Kou, B. Vlastakis, A. Petrenko, K. M. Sliwa, A. Narla, S. Shankar, M. J. Hatridge, M. Reagor, L. Frunzio, R. J. Schoelkopf, M. Mirrahimi, and M. H. Devoret, "Confining the state of light to a quantum manifold by engineered two-photon loss," *Science* **347**, 853–857 (2015). Cited on pages 17, 18, 19, 35 & 36.

27. H. J. Carmichael, *Statistical Methods in Quantum Optics 2: Non-Classical Fields, Theoretical and Mathematical Physics*. Springer Berlin Heidelberg, 2007. Cited on page 18.

28. P. Blasiak, *Combinatorics of boson normal ordering and some applications*. PhD thesis, PhD Thesis, 2005, 2005. Cited on page 19.

29. B. E. A. Saleh and M. C. Teich, *Fundamentals of Photonics*. John Wiley and Sons, New Jersey, USA, 2006. Cited on pages 20 & 36.

30. G. Kirchmair, B. Vlastakis, Z. Leghtas, S. E. Nigg, H. Paik, E. Ginossar, M. Mirrahimi, L. Frunzio, S. M. Girvin, and R. J. Schoelkopf, "Observation of quantum state collapse and revival due to the single-photon Kerr effect," *Nature* **495**, 205–209 (2013), 1211.2228 [quant-ph]. Cited on page 20.

31. M. A. Nielsen and I. L. Chuang, *Quantum Computation and Quantum Information, 10^{th} Anniversary Ed.* Cambridge University Press, New York, 2011. Cited on pages 21, 23 & 24.

32. M. J. Peterer, S. J. Bader, X. Jin, F. Yan, A. Kamal, T. J. Gudmundsen, P. J. Leek, T. P. Orlando, W. D. Oliver, and S. Gustavsson, "Coherence and Decay of Higher Energy Levels of a Superconducting Transmon Qubit," *Physical Review Letters* **114**, 010501 (2015), 1409.6031 [quant-ph]. Cited on page 22.

33. S. H. Autler and C. H. Townes, "Stark Effect in Rapidly Varying Fields," *Physical Review* **100**, 703–722 (1955). Cited on page 23.

34. D. I. Schuster, A. Wallraff, A. Blais, L. Frunzio, R.-S. Huang, J. Majer, S. M. Girvin, and R. J. Schoelkopf, "ac Stark Shift and Dephasing of a Superconducting Qubit Strongly Coupled to a Cavity Field," *Physical Review Letters* **94**, 123602 (2005), cond-mat/0408367. Cited on page 23.

35. A. Sears, *Extending Coherence of Superconducting Qubits: from Microseconds to Milliseconds*. PhD thesis, Yale University, 2013. http://www.eng.yale.edu/rslab/papers/theses/sears.pdf. Cited on page 25.

36. L. Dicarlo, J. M. Chow, J. M. Gambetta, L. S. Bishop, B. R. Johnson, D. I. Schuster, J. Majer, A. Blais, L. Frunzio, S. M. Girvin, and R. J. Schoelkopf, "Demonstration of two-qubit algorithms with a superconducting quantum processor," *Nature* **460**, 240–244 (2009), 0903.2030 [cond-mat.mes-hall]. Cited on page 25.

37. M. D. Reed, L. Dicarlo, S. E. Nigg, L. Sun, L. Frunzio, S. M. Girvin, and R. J. Schoelkopf, "Realization of three-qubit quantum error correction with superconducting circuits," *Nature* **482**, 382–385 (2012), 1109.4948 [quant-ph]. Cited on pages 25 & 26.

38. J. Kelly, R. Barends, A. G. Fowler, A. Megrant, E. Jeffrey, T. C. White, D. Sank, J. Y. Mutus, B. Campbell, Y. Chen, Z. Chen, B. Chiaro, A. Dunsworth, I.-C. Hoi, C. Neill, P. J. J. O'Malley, C. Quintana, P. Roushan, A. Vainsencher, J. Wenner, A. N. Cleland, and J. M. Martinis, "State preservation by repetitive error detection in a superconducting quantum circuit," *Nature* **519**, 66–69 (2015), 1411.7403 [quant-ph]. Cited on page 25.

39. A. D. Corcoles, E. Magesan, S. J. Srinivasan, A. W. Cross, M. Steffen, J. M. Gambetta, and J. M. Chow, "Demonstration of a quantum error detection code using a square lattice of four superconducting qubits," *Nature Communications* **6**, 6979 (2015). Cited on page 25.

40. D. Ristè, S. Poletto, M.-Z. Huang, A. Bruno, V. Vesterinen, O.-P. Saira, and L. Dicarlo, "Detecting bit-flip errors in a logical qubit using stabilizer measurements," *Nature Communications* **6**, 6983 (2015), 1411.5542 [quant-ph]. Cited on page 25.

41. G. Kurizki, P. Bertet, Y. Kubo, K. Mølmer, D. Petrosyan, P. Rabl, and J. Schmiedmayer, "Quantum technologies with hybrid systems," *Proceedings of the National Academy of Sciences* **112**, 3866–3873 (2015). Cited on page 25.

42. X. Zhu, S. Saito, A. Kemp, K. Kakuyanagi, S.-I. Karimoto, H. Nakano, W. J. Munro, Y. Tokura, M. S. Everitt, K. Nemoto, M. Kasu, N. Mizuochi, and K. Semba, "Coherent coupling of a superconducting flux qubit to an electron spin ensemble in diamond," *Nature* **478**, 221–224 (2011), 1111.5399 [quant-ph]. Cited on page 25.

43. Y. Kubo, C. Grezes, A. Dewes, T. Umeda, J. Isoya, H. Sumiya, N. Morishita, H. Abe, S. Onoda, T. Ohshima, V. Jacques, A. Dréau, J.-F. Roch, I. Diniz, A. Auffeves, D. Vion, D. Esteve, and P. Bertet, "Hybrid quantum circuit with a superconducting qubit coupled to a spin ensemble," *Phys. Rev. Lett.* **107**, 220501 (2011). Cited on page 25.

44. M. Reagor, W. Pfaff, C. Axline, R. W. Heeres, N. Ofek, K. Sliwa, E. Holland, C. Wang, J. Blumoff, K. Chou, M. J. Hatridge, L. Frunzio, M. H. Devoret, L. Jiang, and R. J. Schoelkopf, "A quantum memory with near-millisecond coherence in circuit QED," *ArXiv e-prints* (2015), 1508.05882 [quant-ph]. Cited on page 25.

45. K. Stannigel, P. Rabl, A. S. Sørensen, P. Zoller, and M. D. Lukin, "Optomechanical Transducers for Long-Distance Quantum Communication," *Physical Review Letters* **105**, 220501 (2010), 1006.4361 [quant-ph]. Cited on page 25.

46. A. Blais, R.-S. Huang, A. Wallraff, S. M. Girvin, and R. J. Schoelkopf, "Cavity quantum electrodynamics for superconducting electrical circuits: An architecture for quantum computation," *Phys. Rev. A* **69**, 062320 (2004). Cited on pages 25, 32 & 33.

47. A. Wallraff, D. I. Schuster, A. Blais, L. Frunzio, R. S. Huang, J. Majer, S. Kumar, S. M. Girvin, and R. J. Schoelkopf, "Strong coupling of a single photon to a superconducting qubit using circuit quantum electrodynamics," *Nature* **431**, 162–167 (2004). Cited on pages 25 & 32.

48. A. A. Houck, J. A. Schreier, B. R. Johnson, J. M. Chow, J. Koch, J. M. Gambetta, D. I. Schuster, L. Frunzio, M. H. Devoret, S. M. Girvin, and R. J. Schoelkopf, "Controlling the spontaneous emission of a superconducting transmon qubit," *Phys. Rev. Lett.* **101**, 080502 (2008). Cited on pages 25 & 32.

49. M. A. Sillanpaa, J. I. Park, and R. W. Simmonds, "Coherent quantum state storage and transfer between two phase qubits via a resonant cavity," *Nature* **449**, 438–442 (2007). Cited on page 25.

50. J. Majer, J. M. Chow, J. M. Gambetta, J. Koch, B. R. Johnson, J. A. Schreier, L. Frunzio, D. I. Schuster, A. A. Houck, A. Wallraff, A. Blais, M. H. Devoret, S. M. Girvin, and R. J. Schoelkopf, "Coupling superconducting qubits via a cavity bus," *Nature* **449**, 443–447 (2007). Cited on page 25.

51. R. Vijay, D. H. Slichter, and I. Siddiqi, "Observation of quantum jumps in a superconducting artificial atom," *Phys. Rev. Lett.* **106**, 110502 (2011). Cited on pages 25 & 32.

52. M. Hatridge, S. Shankar, M. Mirrahimi, F. Schackert, K. Geerlings, T. Brecht, K. M. Sliwa, B. Abdo, L. Frunzio, S. M. Girvin, R. J. Schoelkopf, and M. H. Devoret, "Quantum back-action of an individual variable-strength measurement," *Science* **339**, 178–181 (2013), http://www.sciencemag.org/content/339/6116/178.full.pdf. Cited on pages 25 & 32.

53. R. M. Foster, "A Reactance Theorem," *Bell System Technical Journal* **3**, 259–267 (1924). Cited on page 27.

54. D. I. Schuster, A. A. Houck, J. A. Schreier, A. Wallraff, J. M. Gambetta, A. Blais, L. Frunzio, J. Majer, B. Johnson, M. H. Devoret, S. M. Girvin, and R. J. Schoelkopf, "Resolving photon number states in a superconducting circuit," *Nature* **445**, 515–518 (2007), cond-mat/0608693. Cited on page 31.

55. I. C. Hoi, C. M. Wilson, G. Johansson, T. Palomaki, B. Peropadre, and P. Delsing, "Demonstration of a single-photon router in the microwave regime," *Phys. Rev. Lett.* **107**, 073601 (2011). Cited on page 32.

56. J. Gambetta, A. Blais, D. I. Schuster, A. Wallraff, L. Frunzio, J. Majer, M. H. Devoret, S. M. Girvin, and R. J. Schoelkopf, "Qubit-photon interactions in a cavity: Measurement-induced dephasing and number splitting," *Phys. Rev. A* **74**, 042318 (2006), cond-mat/0602322. Cited on pages 32 & 33.

57. M. Neeley, R. C. Bialczak, M. Lenander, E. Lucero, M. Mariantoni, A. D. O'Connell, D. Sank, H. Wang, M. Weides, J. Wenner, Y. Yin, T. Yamamoto, A. N. Cleland, and J. M. Martinis, "Generation of three-qubit entangled states using superconducting

phase qubits," *Nature* **467**, 570–573 (2010), 1004.4246 [cond-mat.supr-con]. Cited on page 36.